Fluorescence ratio and photochemical reflectance index as a proxy for photosynthetic quantum efficiency of photosystem II for plants grown at different phosphorus availability.

Sebastian Wieneke[1,2*], Manuela Balzarolo[1,3,4], Han Asard[5], Hamada AbdElgawad[5,6], Josep Peñuelas[3,4], Uwe Rascher[7], Arne Ven[2], Melanie S. Verlinden[2], Ivan A. Janssens[2] & Sara Vicca[2]

[1] Plant and Vegetation Ecology (PLECO), Department of Biology, University of Antwerp, Wilrijk, Belgium

[2] Remote Sensing Centre for Earth System Research (RSC4Earth, Faculty of Physics and Earth Sciences, University of Leipzig, Leipzig, Germany

[3] Consejo Superior de Investigaciones Científicas (CSIC), Global Ecology Unit, CREAF-CSIC-UAB, Bellaterra, 08193 Barcelona, Catalonia, Spain

[4] Centre de Recerca Ecològica i Aplicacions Forestals (CREAF), Cerdanyola del Vallès, 08193 Barcelona, Catalonia, Spain

[5] Integrated Molecular Plant Physiology Research (IMPRES), Department of Biology, University of Antwerp, Antwerp, Belgium.

[6] Botany and Microbiology Department, Faculty of Science, Beni-Suef University, Beni-Suef 62511, Egypt

[7] Institute of Bio- and Geosciences (IBG-2): Plant Sciences, Forschungszentrum Jülich GmbH, Leo-Brandt-Str., Jülich, Germany

Corresponding Author: * Sebastian Wieneke

Email: sebastian.wieneke@uantwerpen.be

Phone: +3232658877

Abstract

Sun-induced chlorophyll fluorescence (SIF) is one of the most promising remote-sensing signals to assess spatio-temporal variation in photosynthesis. Yet, it has been shown that the positive linear relationship of SIF and photosynthesis, often reported from satellite and proximal remote sensing, is mainly driven by the amount of absorbed photosynthetic active radiation (APAR). By normalizing SIF these structural first-order effects can accounted for and SIF is then reflecting physiological regulation of photosynthetic efficiency. However, because of the confounding contribution of non-photochemical energy dissipation, the relationship between SIF and photosynthetic efficiency is non-linear, and therefore additional measurements have to be included to constrain the predictions of photosynthetic efficiency and photosynthetic electron transport (ETR).

We grew *Zea mays* at different phosphorus (P) levels to assess, if P-induced reduction in quantum efficiency of PSII (Φ_{PSII}), can be estimated by the fluorescence efficiency parameters, APAR normalized fluorescence (F_{norm}) and the ratio of the two emitted fluorescence peaks ($F_{\uparrow ratio}$), at leaf level. Results were compared to the photochemical reflectance index (PRI), a well-established index related to the activity of the xanthophyll cycle, a protection mechanism which activates under light-stress conditions. We demonstrate that the relationship between Φ_{PSII} and F_{norm} is non-monotonic across a P limitation gradient, rendering the prediction of Φ_{PSII} by F_{norm} alone unfeasible. The pigment corrected PRI (cPRI) and $F_{\uparrow ratio}$ ($cF_{\uparrow ratio}$), however, share a strong linear relationship with Φ_{PSII}, thereby enabling the estimation of Φ_{PSII}. The possibility to compensate for reabsorption effects on the F_{ratio} at foliar level, as we demonstrate, can help improving Φ_{PSII} and ETR estimations. This may allow improved predictions of photosynthetic light use efficiency parameters without the need of measuring green APAR.

Keywords

quantum efficiency of photosystem II, passive fluorescence, photochemical reflectance index, non-photochemical quenching, phosphorus limitation, photosynthesis, sun-induced fluorescence

Introduction

Accurate monitoring of photosynthesis (gross primary productivity; GPP) is critical for reliable estimates of crop productivity, stress, or failure, as well as for calibration and validation of land surface models (Ciais *et al.*, 2014). Due to its close link to the photosynthetic process, sun-induced fluorescence (SIF) is one of the most promising signals to assess spatio-temporal variation in GPP (Frankenberg *et al.*, 2011; Guanter *et al.*, 2014; Yang *et al.*, 2015). The often observed linear relationship between SIF and GPP from satellite and proximal remote sensing platforms are, however, primarily driven by the amount of absorbed photosynthetic active radiation (APAR) (Miao *et al.*, 2018; Wohlfahrt *et al.*, 2018; Yang *et al.*, 2018; Wieneke *et al.*, 2018; Dechant *et al.*, 2020). It is therefore expected that the relationship of radiation normalized fluorescence and photosynthesis better capture the mechanisms of photosynthesis (Magney *et al.*, 2020; Maguire *et al.*, 2020). Due to canopy effects (e.g. Dechant *et al.*, 2020), but also complex non-linear processes at leaf scale (e.g. van der Tol *et al.*, 2014; Maguire *et al.*, 2020), the interpretation of these relationships is still challenging.

The light energy absorbed by chlorophyll can follow three competitive pathways: drive the photochemical reaction (photochemical quenching), be released as heat (non-photochemical quenching; NPQ), or be emitted as fluorescence in the wavelength range of 650 to 800 nm (F_{tot}) with two distinctive peaks at 685 nm (F_{685}) and 740 nm (F_{740}) (Lichtenthaler & Rinderle, 1988). When exposed to excessive light, plants protect photosystem II (PSII) by releasing energy through NPQ, which consequently reduces photochemical quenching and the quantum efficiency of photosystem II (Φ_{PSII}) (Müller *et al.*, 2001). NPQ and Φ_{PSII} can be derived from pulse amplitude modulated (PAM) fluorometers, which have been used for decades to study photosynthesis at leaf level (Baker, 2008).

Active fluorescence measurements and modeling exercises have shown that the relationship between fluorescence quantum yield and Φ_{PSII} is non-monotonic and driven by changes in NPQ (Maxwell & Johnson, 2000; Baker, 2008; van der Tol *et al.*, 2014;

Maguire *et al.*, 2020). Even though some experiments already indicated the non-monotonic relationship (van der Tol *et al.*, 2014; Pinto *et al.*, 2016; Marrs *et al.*, 2020) there is no study available yet, which combines all relevant confounding factors, i.e. pigment content, quantitative data on photosynthetic efficiency, the degree of non-photochemical dissipation and normalized fluorescence ($F_{norm} = F_{tot}$ / APAR) at leaf level. Due to the complex relationship of F_{norm}, Φ_{PSII} and NPQ and confounding effects of the canopy structure and pigment pools, leaf-level measurements are of utmost importance to improve our understanding about SIF and to establish a functional relationship between SIF and photosynthesis. This is particularly important because SIF is being increasingly used to estimate and interpret photosynthesis in space and time (Wood *et al.*, 2017; Sun *et al.*, 2018; Magney *et al.*, 2019; Mohammed *et al.*, 2019).

Besides Nitrogen, Phosphorus (P) is one of the two major limiting nutrients for terrestrial plant productivity which can result in photosynthetic downregulation (Hou *et al.*, 2021). Previous studies have shown that phosphorus limitation of plants can be tracked by active and passive fluorescence measurements (Conroy *et al.*, 1986; Lima *et al.*, 1999; Yaryura *et al.*, 2009; Frydenvang *et al.*, 2015; Migliavacca *et al.*, 2017; Carstensen *et al.*, 2018). Phosphorus deficiency inhibits adenosine triphosphate (ATP) synthase in the light reactions, leading to excessive proton accumulation in the lumen and activation of the xanthophyll cycle. This, in turn, results in an increase of the energy-quenching (qE) component of NPQ and a subsequent reduction in electron transport rate (ETR) of PSII (Carstensen *et al.*, 2018). While NPQ is controlled by the pH gradient between the lumen and thylakoid, fluorescence is not actively regulated and depends on the relationship between NPQ and qE (Porcar-Castell *et al.*, 2014). The activation of the xanthophyll cycle generates an optical reflectance signal that can be detected around 531 nm. The photochemical reflectance index (PRI) exploits these changes in reflectance at 531 nm, relative to a reference wavelength at 570 nm, to assess the activity of the xanthophyll cycle (Gamon *et al.*, 1992; Peñuelas *et al.*, 1995). The PRI and adaptations thereof are considered as the reflectance indices with the closest link to the degree of NPQ (Garbulsky

et al., 2011; Vicca *et al.*, 2016; Zhang *et al.*, 2017; Kohzuma & Hikosaka, 2018; Woodgate *et al.*, 2019).

The ratio of the two fluorescence peaks ($F_{\uparrow ratio} = F_{\uparrow 685} / F_{\uparrow 740}$) might be another approach for the quantification of Φ_{PSII} from optical remote sensing. While $F_{\uparrow 685}$ is mainly associated with fluorescence emission of PSII, $F_{\uparrow 740}$ consists of fluorescence emission from PSII and PSI (Buschmann, 2007). With increasing P limitation ETR of PSII decreases more strongly than ETR of PSI (Carstensen *et al.*, 2018). Consequently, $F_{\uparrow 685}$ is expected to decrease more than $F_{\uparrow 740}$ leading to an overall decrease of the $F_{\uparrow ratio}$ with increasing P limitation. However, since the $F_{\uparrow ratio}$ is strongly affected by reabsorption features of $F_{\uparrow 685}$ the chlorophyll content has to be taken into account when $F_{\uparrow ratio}$ is calculated (Yaryura *et al.*, 2009; Van Wittenberghe *et al.*, 2013).

In a mesocosm experiment with *Zea mays,* a wide P limitation gradient was created. The goals of this study was to assess how F_{norm}, the PRI and the $F_{\uparrow ratio}$ relate to Φ_{PSII} under increasing P limitation at leaf scale and if F_{norm} and $F_{\uparrow ratio}$ are suitable predictors for Φ_{PSII}. We hypothesized that, i) at leaf level, F_{tot} is not linearly related to photosynthesis under P limitation; ii) in agreement with active fluorescence, F_{norm} and Φ_{PSII} are non-monotonically related; iii) due to its sensitivity to the xanthophyll activity, PRI can be used to estimate Φ_{PSII}; iv) due to the changing contribution of PSII and PSI under P limitation the ratio of the two fluorescence peaks associates with Φ_{PSII}.

Materials and Methods

Experimental setup

Thirty mesocosms (1 m × 1.2 m, 0.6 m high) were set up in a greenhouse in Sint-Katelijne-Waver, Belgium (51.077°N, 4.535°E). The mesocosms were filled with a homogenized, P-poor mixture consisting of pine-forest sand, white river sand, lime and a minority of compost, which was heated at 80 °C for 4 h to ensure the absence of arbuscular mycorrhiza fungi (AMF) (Verlinden *et al.*, 2018), creating a severe P-limiting environment. Each mesocosm was planted with 12 seedlings of maize (*Zea mays* L., variety 'Tom

Thumb') on 21 June 2017 and harvested on 31 August 2017. Whereas all mesocosms received ample nitrogen (95.5 kg N ha^{-1}), potassium (79 kg K ha^{-1}), and all micronutrients (in kg ha^{-1}: 19 Mg, 53 S, 0.4 B, 0.1 Cu, 2.4 Fe, 1.1 Mn, 0.1 Mo, 0.4 Zn), triple superphosphate (TSP) phosphate fertilizer was applied at four levels (2.5, 5, 10 and 20 kg P ha^{-1}) to 20 mesocosms (five replicates each). Plants in these 20 mesocosms were inoculated with AMF (species Rhizophagus irregularis, Symplanta®). Details about the root colonization can be found in Ven *et al.*, 2020 and the supplementary data (Figure S1). TSP was also added at two levels (2.5 and 20 kg P ha^{-1}) to 10 mesocosms without AMF inoculation. Because AMF are especially important in plant P uptake from soils (Marschner *et al.*, 1986; Ge *et al.*, 2000; Liao *et al.*, 2001), we assumed that P deficiency would be most extreme in the non-AMF treatments. Above- and below ground total dry biomass (TB), as well as the carbon (C), nitrogen (N) and P contents of the plant tissues (roots, stems, leaves and cobs) were measured after harvest (71 days after seeding) (Ven *et al.*, 2020).

Volumetric soil-water content was monitored (CS650, Campbell Scientific Inc., Logan, USA) in all mesocosms and maintained at a non-limiting (6-12%) level by manual irrigation. Per mesocosm two recently matured sunlit leaves were selected in each of two measurement campaigns, 27-29 and 57-61 days after seeding (first and second campaigns, respectively). We first measured the CO_2 gas exchange and active fluorescence and then passive fluorescence and reflectance (R) for each selected leave. Finally, the leaves were frozen in liquid nitrogen and analyzed for Chlorophyll a and b, beta-Carotene, and the xanthophyll-cycle pigments Violaxanthin, Antheraxanthin and Zeaxanthin (Balzarolo *et al.*, 2018). From the 120 leaf measurements 16 were discarded due to errors in the spectral measurement sequence (measurements with wrong or no short-pass filter) and bad data quality of the gas measurements due to a gasket air leakage.

Measurement of foliar gas exchange and active fluorescence

Foliar CO_2 gas exchange, light response curves and active fluorescence were measured using a portable gas exchange system (LI-6400, LI-COR, Lincoln, NE, USA) operating with a leaf chamber fluorometer (LI-6400-40). Air flow rate and CO_2 concentration in the leaf cuvette was maintained at 400 µmol mol^{-1} and the block temperature was set at 20°C. Net leaf photosynthesis (A_{net}) and steady-state fluorescence (F_s) were measured at a fixed photosynthetic photon flux density (I) value of 1000 µmol s^{-1} m^{-2}, while the net CO_2 exchange at zero light was considered as leaf dark respiration (R_d). Gross photosynthesis (A_g) was calculated as:

$$A_g = A_{net} + R_d \quad \text{(E1)}$$

Photosynthetic light response curves were obtained at light intensities of 0, 20, 50, 100, 250, 500, 1000, 1500 µmol m^{-2} s^{-1} (c.f. Figure S2). The photochemical yield of PSII (Φ_{PSII}), the fraction of absorbed photons by PSII that are used for photochemistry, was inferred from active fluorescence measurements and computed as in Genty *et al.* (1989):

$$\Phi_{PSII} = \left(\frac{F_m{}' - F_s}{F_m{}'}\right) \quad \text{(E2)}$$

the maximal fluorescence of the light adapted leaf ($F_m{}'$) was obtained by triggering it with a saturating light flash.

Analysis of foliar pigments

Frozen maize leaves were homogenized using a MagNALyser (Roche Diagnostics, Vilvoorde, Belgium) in acetone. The solution was centrifuged (14 000 g, 4 °C, 20 min), and the supernatant filtered (Acrodisc GHP filter, 0.45 µm 13 mm), and analyzed by high-performance liquid chromatography HPLC (Shimadzu SIL10-ADvp, reversed-phase, at 4 °C) (Thayer & Björkman, 1990). Carotenoids (Car) were separated on a silica-based C18 column (Waters Spherisorb, 5 µm ODS1, 4.6 × 250 mm, with solvent A 81:9:10 acetonitrile:methanol:water and solvent B 68:32 methanol:ethyl acetate. Chlorophyll a and b, beta-carotene and xanthophyll's were detected using a diode-array detector

(Shimadzu SPD-M10Avp) at four wavelengths (420, 440, 462, 660 nm). Concentrations were determined using the Shimadzu Lab Solutions Lite software, and a calibration curve (Balzarolo *et al.*, 2018).

The epoxidation state (EPS) of the xanthophyllic pigments, a group of carotenoid pigments (Violaxanthin, V; Antheraxanthin, A; Zeaxanthin, Z) which are involved in the heat dissipation mechanism of the pH- or energy-dependent form of non-photochemical quenching (qE) was calculated as:

$$EPS = \frac{\left(V + \frac{A}{2}\right)}{(V + A + Z)} \quad \text{(E3)}$$

For plants containing VAZ pigments, excessive light conditions lead to proton accumulation within the chloroplast lumen, resulting in its acidification and the activation of the xanthophyllic cycle. By de-epoxidating the diepoxide violaxanthin via the monoepoxide antheraxanthin to the epoxide-free form zeaxanthin, excessive energy can be released as heat. Hence, low values of EPS indicate high qE activity and thus plants emit more energy as heat and reduce their Φ_{PSII}.

Measurement of passive foliar fluorescence and reflectance

After measuring gas exchange and active fluorescence, maize leaves were cut and passive fluorescence and reflectance were immediately measured using a FluoWat leaf clip (for a detailed description c.f. Van Wittenberghe *et al.*, 2013) connected to a spectroradiometer (spectral resolution: 3 nm, spectral range: 325–1075 nm, ASD FieldSpec, Malvern Panalytical, Boulder, USA). The FluoWat leaf clip was carefully positioned over the same area of the leaf where gas exchange was measured. The design of the FluoWat allows observing the leaf at the nadir from upward and downward positions, where the light falls on the leaf at 45°. Reflectance (R) and transmittance (T) were measured using upward and downward fiber-optic insertions. A short-pass filter that blocks light at wavelengths >650 nm was moved in front of the incident light to obtain upward and downward emitted F ($F_{\uparrow}$ and $F_{\downarrow}$, respectively). Due to cloudy weather conditions during both

campaigns, the FluoWat was used in combination with an artificial light source (ASBN-W, Spectral Products, Connecticut, Putnam, USA; PPFD of 596±28.9 µmol m^{-2} s^{-1}). To allow a comparison of Φ_{PSII} measurements (performed at 1000 µmol m^{-2} s^{-1}) with passive fluorescence (performed at 600 µmol m^{-2} s^{-1}), a transfer function derived from campaign- and treatment- specific light response curves (c.f. Figure S2), was used to recalculate Φ_{PSII} to 600 µmol m^{-2} s^{-1}. These values where then used for the subsequent analysis.

Reflectance, transmittance and F are thus obtained for the same area of the leaf in one measurement cycle (Van Wittenberghe *et al.*, 2013). The photochemical reflectance index (PRI) for the acquired foliar-reflectance spectra was calculated as:

$$PRI = \frac{R_{570} - R_{531}}{R_{570} + R_{531}} \quad \text{(E4)}$$

where the reflectance of green leaves at 531 nm (R_{531}) can be related to the EPS of the xanthophyll cycle and the reflectance at 570 nm (R_{570}) is utilized as a reference wavelength (Gamon *et al.*, 1992). We used the original PRI equation (E4) where an increased PRI indicates an increased release of excess energy by the energy- or pH-dependent (qE) component of non-photochemical quenching (NPQ). Where non-photochemical quenching is composed of qE, photoinhibition (qI) and state-transition (qT):

$$NPQ = qE + qI + qT \quad \text{(E5)}$$

To avoid negative PRI values, scaled PRI (sPRI) (Rahman *et al.*, 2004) was calculated as:

$$sPRI = \frac{(PRI + 1)}{2} \quad \text{(E6)}$$

Several studies reported that seasonal changes in foliar pigments affect the relationship between PRI and non-photochemical quenching (Peñuelas *et al.*, 1997; Gamon *et al.*, 2001; Sims & Gamon, 2002; Filella *et al.*, 2009; Rahimzadeh-Bajgiran *et al.*, 2012; Gitelson *et al.*, 2017a). Wong & Gamon (2015) showed that that the PRI changes linearly with the ratio of carotene (Car) to total chlorophyll (Chl). Since this may lead to misinterpretation of PRI as an indicator of qE (Gitelson *et al.*, 2017b; Alonso *et al.*, 2017), we corrected sPRI (cPRI) by normalizing for the carotene to total chlorophyll ratio (Car:Chl).

$$cPRI = \frac{sPRI}{Car{:}\,Chl} \quad \text{(Error! Bookmark not defined.E7)}$$

Two different cPRI where calculated: one based on the measured foliar pigments (cPRI, E7), and another where Car:Chl was based on a vegetation index ($cPRI_{vi}$). We tested the performance of several vegetation indices in predicting Car:Chl (c.f. Table S2) and found that an adapted version of the CCRI (Zhou *et al.*, 2019; Gitelson, 2020) performed best (R^2 = 0.60, c.f. Figure S5c). In its original version the CCRI is calculated as a ratio of the carotenoid index CARI = $(R_{720}-R_{521})/R_{521}$ (Zhou *et al.*, 2017) and the red edge chlorophyll index $CI_{red\text{-}edge}$ = $(R_{780\text{-}800}/R_{700})$-1 (Gitelson *et al.*, 2003). While in this study the $CI_{red\text{-}edge}$ showed a strong correlation with Chl (R^2 = 0.98, c.f. Figure S5a), we found that the red-edge carotenoid index $CAR_{red\text{-}edge}$ = $((R_{510})^{-1} - (R_{700})^{-1})\cdot R_{770}$ (Gitelson *et al.*, 2006) performed best in estimating the observed relatively low carotenoid contents (R^2 = 0.89, c.f. Figure S5b, Table S2). Accordingly, the adapted CCRI (aCCRI) was calculated as:

$$aCCRI = \frac{CAR_{red-edge}}{CI_{red-edge}} \quad \text{(Error! Bookmark not defined.E8)}$$

The total amount of fluorescence emitted by the leaf (F_{tot}, W m^{-2} sr^{-1}) in a wavelength from 650 to 800 nm was calculated as:

$$F_{tot} = F_{\uparrow} + F_{\downarrow} \quad \text{(E9)}$$

F efficiency (F_{norm}, %), was derived by normalizing F_{tot} by APAR (the product of photosynthetically active radiation between 400 and 700 nm (PAR, W m^{-2}) and the fraction of PAR absorbed by the leaf (α_{leaf}), W m^{-2}) to improve comparison of the measurements:

$$F_{norm} = \frac{F_{tot} \cdot \pi}{fPAR \cdot PAR} \cdot 100 \quad \text{(E10)}$$

where PAR was derived from white reference measurements. Since the Teflon based white reference is not 100% reflective and a fraction of the light is transmitted (around 5%), we corrected PAR by accounting for the white reference transmittance measured for each white reference measurement cycle. fPAR was calculated as:

$$fPAR = 1 - R - T \quad \text{(E11)}$$

To compare the contribution of $F_{\uparrow}$ to total F ($F_{\uparrow\%}$, %) under changing P limitation, $F_{\uparrow\%}$ was calculated as:

$$F_{\uparrow\%} = \frac{F_{\uparrow}}{(F_{\uparrow} + F_{\downarrow})} \cdot 100 \quad \text{(E12)}$$

Semi mechanistic model for estimating Φ_{PSII} by $cF_{\uparrow ratio}$

The peak ratio of fluorescence emitted by the adaxial surface of the leaf ($F_{\uparrow ratio}$) was calculated as:

$$F_{\uparrow \mathrm{ratio}} = \frac{F_{\uparrow 685}}{F_{\uparrow 740}} \quad \text{(E13)}$$

Where the first peak of fluorescence is located at 685 nm ($F_{\uparrow 685}$) and the second peak at 740 nm ($F_{\uparrow 740}$). To compensate for chlorophyll related reabsorption effects of $F_{\uparrow 685}$ a corrected $F_{\uparrow ratio}$ ($cF_{\uparrow ratio}$) was calculated as:

$$cF_{\uparrow \mathrm{ratio}} = \frac{F_{\uparrow 685} \cdot cf}{F_{\uparrow 740}} \quad \text{(E14)}$$

Where the correction factor (cf) was calculated from the exponential relationship (R^2 = 0.88) between leaf transmittance in the red (T_{685}) and the vegetation index $CI_{red\text{-}edge}$:

$$cf = \frac{1}{0.02 + 0.0003 \cdot CI_{red-edge}{}^{-2.2}} \quad \text{(E15)}$$

To evaluate if the relationship between Φ_{PSII} and the $cF_{\uparrow ratio}$ is affected by their covariation with Chl, a partial correlation was used to determine the strength of their linear relationships while controlling for the Chl content as the covariate.

Statistical analysis

Data normality and homoscedasticity were verified using Shapiro-Wilk and Levene tests, respectively. A two-way analysis of variance (ANOVA) was applied to determine if the variables differed between treatments and campaigns, where non-normally distributed parameters were log-transformed. A Tukey post hoc test was applied for pairwise comparison when the effects of a factor were significant.

The statistical analysis was performed in Python, using the packages pandas (McKinney, 2010), numpy (Harris *et al.*, 2020), scipy (Virtanen *et al.*, 2020) and sklearn (Pedregosa *et al.*, 2011).

Results

Biomass distribution and foliar N:P ratio at the end of the season

Total biomass (TB) at the end of the experiment indicated that P limitation strongly affected plant growth: as P supply declined, TB decreased exponentially (Figure 1a). The treatments with lowest P and no AMF (P1S) showed the lowest biomass and several plants in these mesocosms died prematurely (i.e., before producing seeds). The more than 50% reduction in the P4S treatment (relative to P4) highlights the importance of AMF for these plants, even under well-fertilized conditions. Foliar N:P ratios stabilized near 7 for all mesocosms with active AMF, but were much higher for the mesocosms without AMF (≈ 14 and 21 for P4S and P1S, respectively) (Figure 1b), indicating increased P shortage.

Because several plants in P1S senesced and died prematurely, we omitted the P1S treatment from the biomass distribution analysis (Figure 1c).

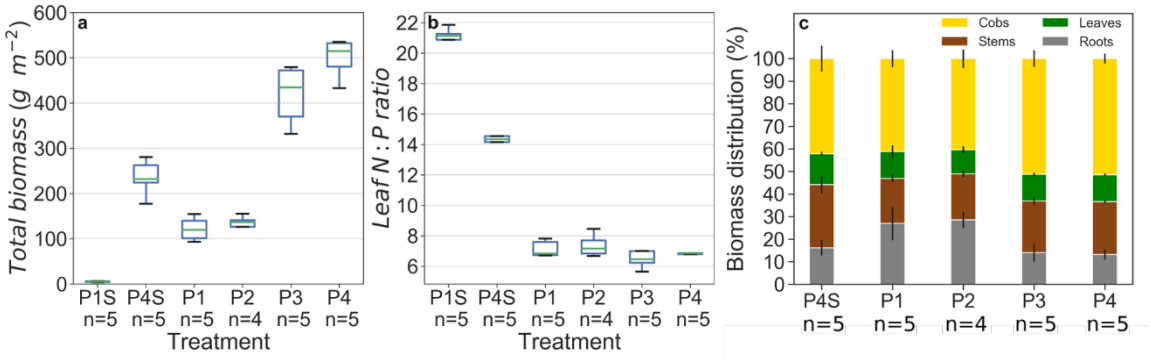

Figure 1: Total biomass (a), foliar N:P ratio (b) and biomass distribution (c) of the maize plants at harvest. P1, P2, P3 and P4 indicate treatment with 2.5, 5, 10 and 20 kg P ha^{-1} triple superphosphate, respectively. P1S and P4S were pasteurized to ensure the absence of arbuscular mycorrhizal fungi. Sample size is indicated by n.

Composition of foliar pigments under P limitation

All foliar pigment contents exhibited the same patterns in both campaigns. Chl a&b, beta-carotene and VAZ contents during the first campaign were higher for the highest P-fertilization treatments (P3, P4 & P4S) and the lowest for the lowest P-fertilization treatments (P1, P2 & P1S) (Figure 2a & Figure S3a, b, c, d). Foliar pigment concentrations during the second campaign were significantly lower in the pasteurized mesocosms (P4S & P1S) than in their AMF inoculated counterparts with low- (P1 & P2) and, in particular, high P fertilization (P3 & P4) (Figure 2e & Figure S3e, f, g, h). In both campaigns the Car:Chl ratio increased with P fertilization (Figure 2b&f), but with overall higher values during the second campaign. The Chl content of P1 and P2 showed no significant difference with each other in both campaigns. However an increase in the Car:Chl and VAZ:Chl ratio was observed for P2 compared to P1, indicating a stronger investment into carotenoids (Figure 2a, b, e, f). The ratio between the contents of xanthophyll and Chl pigments in both campaigns was the lowest in the pasteurized mesocosms and increased with increasing P fertilization (Figure 2c & g). During the first campaign also the epoxidation state (EPS) increased with the increasing rate of P fertilization and AMF presence (Figure

320 2d). EPS during the second campaign was very high (except for P1S), with low variability
321 among treatments (Figure 2h).
322

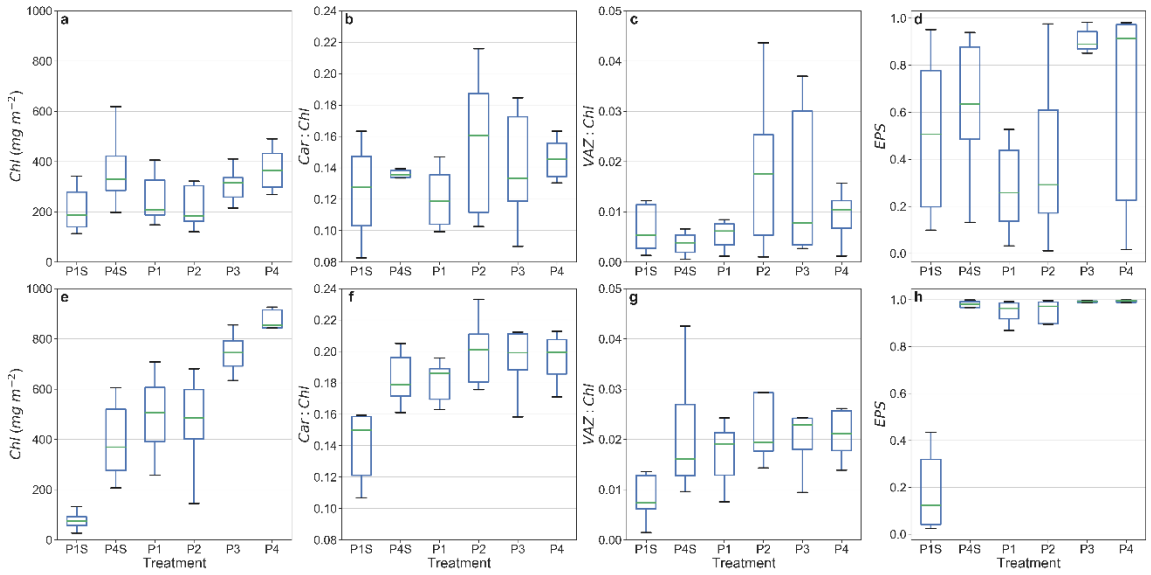

Figure 2: Box plots of total chlorophyll content, the ratio between beta-carotene and total chlorophyll, the ratio of the total xanthophyll pigment (VAZ) content to total chlorophyll and the epoxidation state (EPS) 27-29 days after seeding (DAS, first campaign) a-d, and 57-61 DAS (second campaign) e-h. P1, P2, P3 and P4 indicate treatment with 2.5, 5, 10 and 20 kg P ha^{-1} triple superphosphate, respectively. P1S and P4S were pasteurized to ensure the absence of arbuscular mycorrhizal fungi.

Photosynthesis and $F_{\uparrow\%}$ under P limitation

Our experiment produced a wide range of leaf photosynthesis (A_g) and photochemical yield of PSII (Φ_{PSII}) values, which varied strongly among treatments. During the first campaign, A_g and Φ_{PSII} were higher in the high P fertilization treatments (P3, P4 & P4S) than in the low P fertilization treatments (P1, P2 & P1S) (Figure 3a, b). A different pattern appeared during the second campaign, in which A_g and Φ_{PSII} were similar across all treatments with AMF (P1 to P4), but were significantly lower in the absence of AMF (P4S & P1S versus P1 to P4) (Figure 3e, f).

During the first campaign fPAR was relatively similar across treatments and only during the second campaign a treatment effect emerged; fPAR then decreased with increasing P limitation and decreasing total chlorophyll content (Figure 3d, h). $F_{\uparrow\%}$ declined from around 65% to 50% with increasing P limitation. During the second campaign, treatment

differences had disappeared in the presence of AMF, while the treatments without AMF still exhibited low $F_{\uparrow\%}$ (Figure S4).

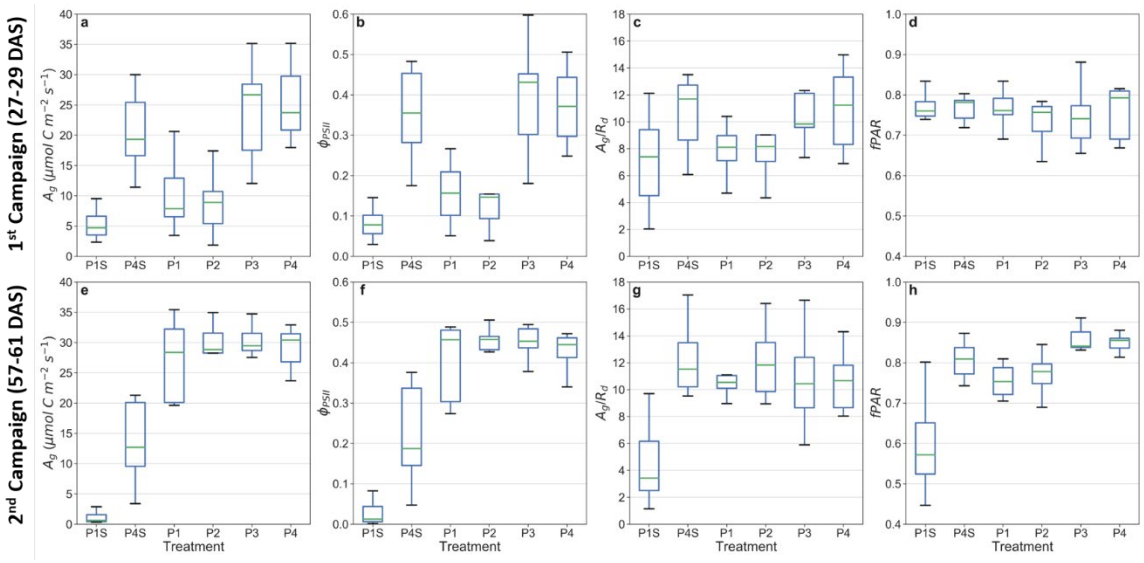

Figure 3: Box plots of gross photosynthesis (Ag), quantum efficiency of PSII (ΦPSII)), ratio of Ag to dark respiration (Rd) and the fraction of absorbed photochemical active radiation (fPAR). 27-29 days after seeding (DAS, first campaign) a-d, and 57-61 DAS (second campaign), e-h. P1, P2, P3 and P4 indicate treatment with 2.5, 5, 10 and 20 kg P ha^{-1} triple superphosphate, respectively. P1S and P4S were pasteurized to ensure the absence of arbuscular mycorrhizal fungi.

Estimation of EPS by cPRI

Across treatments and campaigns, EPS showed a strong positive relationship with Φ_{PSII} (Figure 4a). The scaled PRI (sPRI) showed a strongly decreasing linear relationship with EPS (Figure 4b), where the Car:Chl normalized sPRI (cPRI) greatly improved the prediction of EPS, with R^2 = 0.82 and a *rRMSE* = 13.3%. Compared to the performance of sPRI the reflectance based $cPRI_{vi}$ was also a better predictor of EPS, albeit less than cPRI (Figure 4). The partial correlation of EPS, Car:Chl, sPRI, cPRI and $cPRI_{vi}$ showed that the relationship between EPS and sPRI was strongly affected by the Car:Chl ratio. The Car:Chl ratio had,

361 however, considerably less effect on the relationship between cPRI, $cPRI_{vi}$ and EPS (Table
362 S4).
363

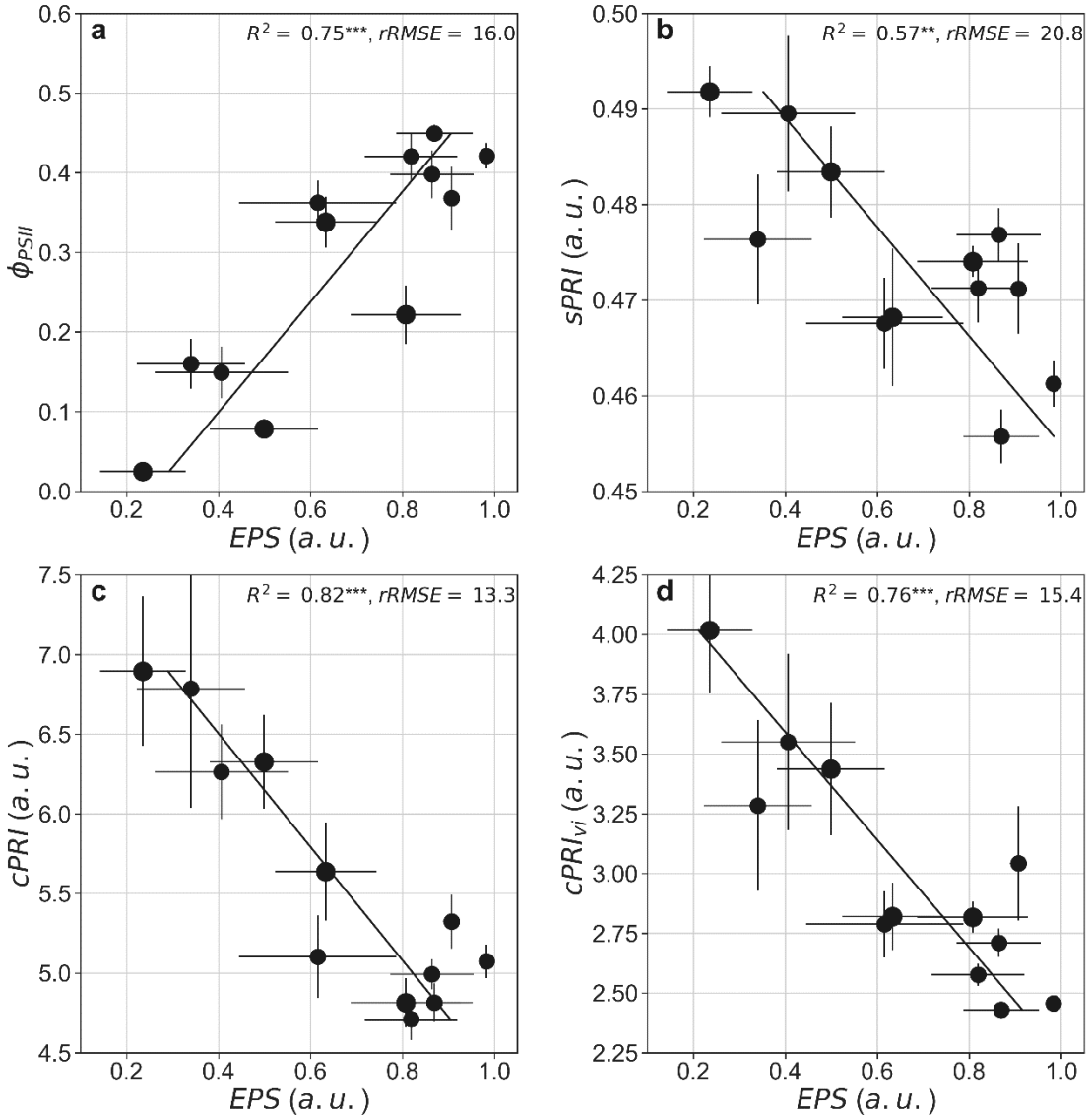

364

365 *Figure 4: (a) Relationship between epoxidation state (EPS) and photochemical yield of PSII (Φ_{PSII}). (b)*
366 *Relationship between EPS and scaled photochemical reflectance index (sPRI). (c) Relationship between EPS*
367 *and corrected sPRI. cPRI was calculated by normalizing the sPRI by the measured foliar pigment ratio of*
368 *carotene to chlorophyll concentrations. (d) Relationship between EPS and $cPRI_{vi}$. $cPRI_{vi}$ was normalized by a*
369 *vegetation index derived ratio of carotene to chlorophyll. EPS and PRI are given in arbitrary units (a.u.). The*
370 *black line represents the best fitting model for all treatments for both campaigns. The asterisks indicate the*
371 *significance level (** = P ≤ 0.01, *** = P ≤ 0.001). Number of samples per treatment for Campaign 1: P1 = 5,*
372 *P2 = 5, P3 = 7, P4 = 5, P1S = 9, P4S = 8. Number of samples per treatment for Campaign 2: P1 = 10, P2 = 9,*
373 *P3 = 10, P4 = 10, P1S = 9, P4S = 10.*

Estimation of photosynthesis by fluorescence and reflectance indices

No significant linear relationship was found between gross leaf photosynthesis (A_g) and total fluorescence (F_{tot}) along the P limitation gradient (Figure 5a), even when the highly stressed P1S treatment of the second campaign (point with lowest A_g value) is excluded. Due to the constant light conditions of the Li-6400, Φ_{PSII} showed a strong linear relationship with A_g (Figure 5b).

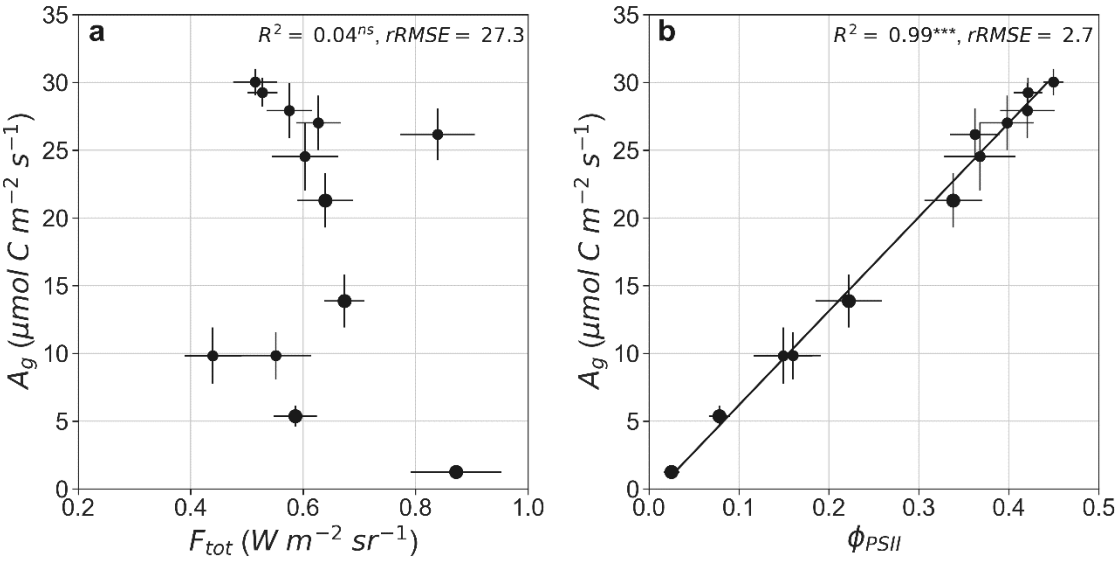

*Figure 5: a) Relationship between foliar gross photosynthesis (Ag) and total fluorescence (F_{tot}; fluorescence emitted between 650-800nm emitted from upper and lower side of the leaf). b) Relationship between foliar gross photosynthesis (A_g) and photochemical yield of PSII (Φ_{PSII}). The asterisks indicate the significance level (** = P ≤ 0.01, *** = P ≤ 0.001). Number of samples per treatment for Campaign 1: P1 = 5, P2 = 5, P3 = 7, P4 = 5, P1S = 9, P4S = 8. Number of samples per treatment for Campaign 2: P1 = 10, P2 = 9, P3 = 10, P4 = 10, P1S = 9, P4S = 10.*

The relationship between Φ_{PSII} and F_{norm}, as well as between $cPRI_{vi}$ and F_{norm}, were best described by a 3th-degree polynomial (Figure 6a&b). When Φ_{PSII} was low (<0.13) and cPRI high (>3.5), F_{norm} showed the highest values (ca. 1.6 %), but decreased quickly with increasing Φ_{PSII} and decreasing $cPRI_{vi}$. As Φ_{PSII} further increased (>0.13) and $cPRI_{vi}$ decreased (<3.5), F_{norm} increased, leading to a positive linear relationship (Figure 6a) with Φ_{PSII} and a negative linear relationship with $cPRI_{vi}$. As Φ_{PSII} exceeded 0.31 and $cPRI_{vi}$

decreased further (<2.9), F_{norm} decreased again to its lowest values (0.6%), suggesting a negative linear relationship with Φ_{PSII} and a positive relationship with $cPRI_{vi}$ (Figure 6a&b). The relationship between $cPRI_{vi}$ and Φ_{PSII} on the other hand showed a strong linear relationship (Figure 6c).

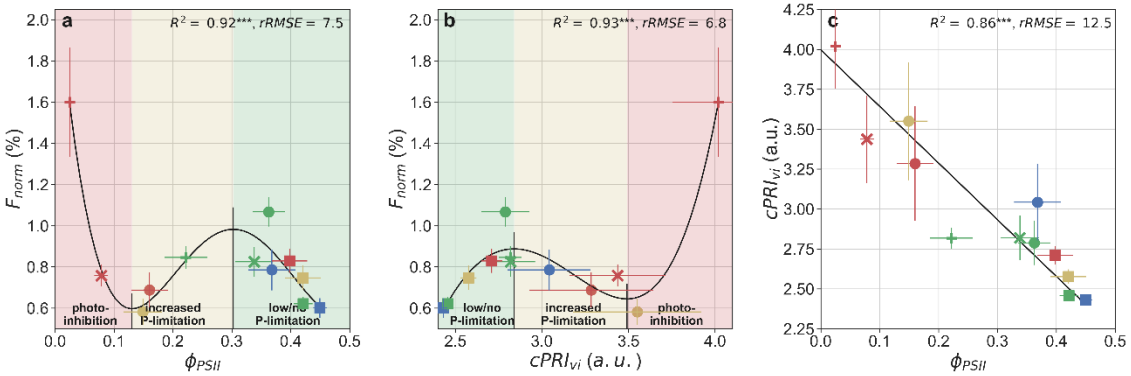

*Figure 6: (a) Relationship between normalized fluorescence (F_{norm}; total fluorescence emitted between 650-800nm emitted from upper and lower side of the leaf divide by absorbed photosynthetic active radiation) and photochemical yield of PSII (Φ_{PSII}). The black line represents the best fitting polynomial model for all treatments for both campaigns. The green, yellow and red lines represent the best fitting linear models for all treatments under low P limitation, increasing P limitation and the highest stress conditions, respectively. The black horizontal line indicates the local minima and maxima of the polynomial model. (b) Relationship between F_{norm} and $CAR_{red\text{-}edge}$:$CI_{red\text{-}edge}$ ratio normalized scaled photochemical reflectance index ($cPRI_{vi}$). cPRI is given in arbitrary units (a.u.). The green, yellow and red background color represent the P stress level (green = low/no P stress, yellow = increased P stress, red = photoinhibition). The black line represents the best fitting polynomial model for all treatments for both campaigns. The black horizontal line indicates the local minima and maxima of the polynomial model. (c) Relationship between $cPRI_{vi}$ and Φ_{PSII}. Colors represent the phosphor treatments (green, P4; blue, P3; yellow, P2; red, P1), where the circles represent the first campaign and squares the second campaign. The x symbol represents treatments without arbuscular mycorrhizal fungi (AMF) of the first campaign, the plus symbol treatments without AMF of the second campaign. The asterisk indicate the significance level (** = P ≤ 0.01, *** = P ≤ 0.001). Number of samples per treatment for Campaign 1: P1 = 5, P2 = 5, P3 = 7, P4 = 5, P1S = 9, P4S = 8. Number of samples per treatment for Campaign 2: P1 = 10, P2 = 9, P3 = 10, P4 = 10, P1S = 9, P4S = 10.*

As P limitation intensified and Φ_{PSII} decreased, the $F_{\uparrow ratio}$ decreased linearly and reached its lowest point at Φ_{PSII} around 0.25. The relationship was then reversed and $F_{\uparrow ratio}$ increased with increasing Φ_{PSII} (Figure 7a). The transmittance at 685 nm (TR_{685}) decreased

exponentially with increasing $CI_{red-edge}$ (R^2 = 0.94, rRMSE = 6.3%) (Figure 7b). The correction of $F_{\uparrow ratio}$ for reduced reabsorption effects under P limitation ($cF_{\uparrow ratio}$, c.f. E14) resulted in a strong linear relationship between $cF_{\uparrow ratio}$ and Φ_{PSII} (Figure 7c). The correlation of Φ_{PSII} with Chl, $CI_{red-edge}$ and $cF_{\uparrow ratio}$ showed that Φ_{PSII} correlated stronger with $cF_{\uparrow ratio}$ than with Chl or $CI_{red-edge}$. When controlled for Chl and $CI_{red-edge}$ the partial correlation of $cF_{\uparrow ratio}$ to Φ_{PSII} was still higher than the correlation between Chl and $CI_{red-edge}$ to Φ_{PSII} (Table 1).

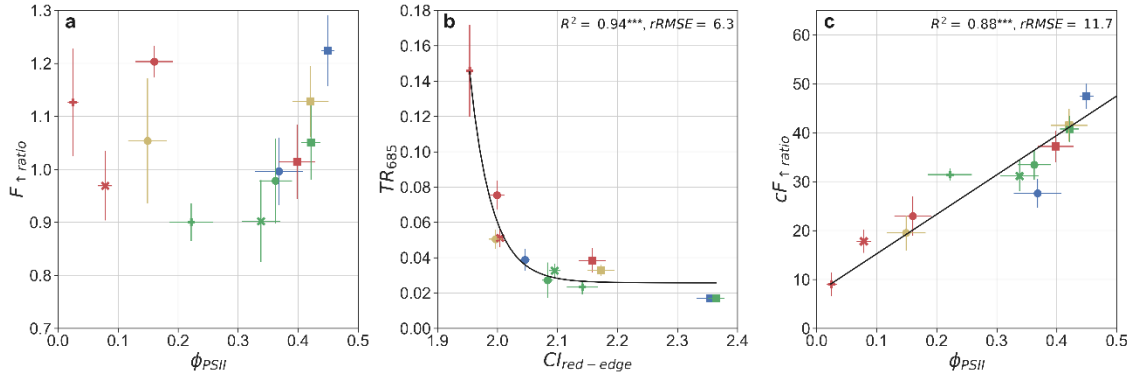

*Figure 7: a) Relationship between the peak ratio of fluorescence ($F_{\uparrow ratio} = F_{\uparrow 685} / F_{\uparrow 740}$) and photochemical yield of PSII (Φ_{PSII}). The red line indicates treatments where the relationship between $F_{\uparrow ratio}$ and Φ_{PSII} is mainly driven by decreasing reabsorption effects, the dark blue line indicates treatments where their relationship between $F_{\uparrow ratio}$ and Φ_{PSII} is mainly driven by increased contribution of PSI (relative increase in $F_{\uparrow 740}$). b Relationship between the foliar transmittance at 685 nm (TR_{685}) and total Chlorophyll (Chl). The black line represents the best fitting model for all treatments for both campaigns. c) Relationship between chlorophyll normalized $F_{\uparrow ratio}$ ($cF_{\uparrow ratio}$) and Φ_{PSII}. The black line represents the best fitting model for all treatments for both campaigns. Colors represent the phosphor treatments (red: P1, yellow: P2, blue: P3, green: P4), where the circles represent the first campaign and squares the second campaign. The x symbol represent treatments without arbuscular mycorrhizal fungi (AMF) of the first campaign, the plus symbol treatments without AMF of the second campaign. The asterisk indicate the significance level (** = P ≤ 0.01, *** = P ≤ 0.001). Number of samples per treatment for Campaign 1: P1 = 5, P2 = 5, P3 = 7, P4 = 5, P1S = 9, P4S = 8. Number of samples per treatment for Campaign 2: P1 = 10, P2 = 9, P3 = 10, P4 = 10, P1S = 9, P4S = 10.*

*Table 1: Pearson correlation coefficient (r) of the partial correlation analysis of Φ_{PSII}, Chl, $CI_{red-edge}$, $cF_{\uparrow ratio}$ and $cPRI_{vi}$. The asterisk indicate the two-tailed significance level (^{ns} = P > 0.05, * = P ≤ 0.05, ** = P ≤ 0.01, *** = P ≤ 0.001).*

		Correlation with Φ_{PSII}			
		$cF_{\uparrow ratio}$	$cPRI_{vi}$	Chl	$CI_{red-edge}$
Control variables	none	0.936***	- 0.927***	0.778**	0.782**
	Chl	0.844***	-0.807**	-	-
	$CI_{red-edge}$	0.847***	-0.800**	-	-

Discussion

Plant response to P limitation

The aim of the current study was to create different levels of P shortage, which would allow us to assess the suitability of F, F_{norm}, F_{ratio} and PRI as proxies for photosynthetic activity along the wide gradients in A_g and Φ_{PSII}. The experiment was successful in creating these gradients. Detailed information about plant response to P limitation of this experiment can be found in Ven *et al.* (2020).

Implications for remote sensing of Φ_{PSII} by PRI

Our results show that sPRI can be used to estimate P deficiency effects on foliar EPS because of its relationship to the energy- (or pH-) dependent mechanism of non-photochemical quenching. The foliar pigment content, however, exert a dominant influence on the sPRI (Zhang *et al.*, 2011; Garbulsky *et al.*, 2011; Gitelson *et al.*, 2017b), and therefore methods to minimize these confounding effects are needed. We were able to improve the estimation of leaf-level EPS and Φ_{PSII} by normalizing the sPRI by the Car:Chl ratio. We further showed that alternatively to the measured pigment pools, remotely sensed indices of chlorophyll and carotenoids can be used to correct the PRI at leaf level.

462 Even though studies have generally found that PRI can be related to leaf photosynthetic
463 processes in specific ecosystems (Peñuelas *et al.*, 2011; Porcar-Castell *et al.*, 2012), a
464 universal or standardized method linking PRI to non-photochemical quenching or
465 photosynthesis at top of canopy is still lacking (Gitelson *et al.*, 2017b; Alonso *et al.*, 2017).
466
467 **Implications for remote sensing of Φ_{PSII} by SIF**
468 Results confirmed our first hypothesis that F_{tot} is not linearly related to leaf
469 photosynthesis (A_g) across a P limitation gradient. We show that the relationship of the
470 physiologically linked parameters Φ_{PSII} and F_{norm} was best described by a 3^{th}-degree
471 polynomial across the P gradient, which confirmed our second hypothesis. This pattern
472 was previously reported from active and passive fluorescence measurements under heat
473 stress conditions (Magney *et al.*, 2017) and active fluorescence measurements and model
474 exercises (van der Tol *et al.*, 2014). The latter have shown that F_{norm} is strongly influenced
475 by the predominant NPQ protective mechanism and that an increase in NPQ can change
476 the typically negative relationship between Φ_{PSII} and F_{norm} into a positive relationship.
477 F_{norm} can thus increase under extreme irradiance stress conditions, when photoinhibition
478 occurs and Φ_{PSII} is strongly downregulated while non-photochemical quenching is the
479 highest (van der Tol *et al.*, 2014), as it was the case in our experiment. The polynomial
480 relationship complicates the estimation of Φ_{PSII} from F_{norm}, because F_{norm} can be
481 misinterpreted if the stress stage, and consequently the corresponding relationship, is
482 unknown. Even though the $cPRI_{vi}$ to F_{norm} relationship could be used to detect the stress
483 phases, it is more intuitive to estimate Φ_{PSII} on the basis of its strong linear relationship
484 with $cPRI_{vi}$. We thereby confirm our third hypothesis that due to its sensitivity to the
485 xanthophyll activity, cPRI and $cPRI_{vi}$ can be used to estimate Φ_{PSII}.
486 While the breakpoint at local minima can be attributed to severe photoinhibition, the
487 light response curves indicate that the breakpoint at local maxima is caused by a switch
488 from light to RuBisCO limitation due to increasing P limitation. The treatment-specific
489 light response curves shown in Figure S2, indicate that observations under low P limitation

(campaign 1: P3,P4 and campaign 2: P1, P2, P3, P4, P4S) (Figure 6a) were light-limited during the measurements (APAR values around 450-500 mmol m^{-2} s^{-1}). In contrast, the treatments with increased P limitation on the left side of the local maxima (campaign 1: P1, P2, P1S, P4S and campaign 2: P1S) (Figure 6a) might have been limited by an insufficient amount of RuBisCO (Figure S2).

These findings may also clarify why satellite and in-situ canopy measurements rarely capture the right side of the local maxima, where F_{norm} and photosynthesis share a negative relationship. SIF products derived from satellite observations have a local overpass time of 9:30 (GOME2) or 13:30 (OCO-2, TROPOMI). At this time of day, and under clear sky conditions (a prerequisite to obtain satellite images), photosynthesis might not be light-limited, in particular during the growing season. Thus, satellite SIF products might only represent the left side (RuBisCO -limited) of the local maxima, where SIF correlates positively with photosynthesis. Even though in-situ canopy measurements could theoretically track SIF under low light conditions, these measurements are rare, since they are normally discarded due to increased uncertainties in the retrieval of SIF under low solar angles or cloudy conditions (Meroni *et al.*, 2009).

Previous research showed that increasing P limitation decreases ETR of PSII more than ETR of PSI (Carstensen *et al.*, 2018). This can lead to a stronger decrease in $F_{\uparrow 685}$ than in $F_{\uparrow 740}$ (Buschmann, 2007). Therefore, the $F_{\uparrow ratio}$ might offer an alternative approach allowing the estimation of photosynthetic efficiency from optical remote sensing. With increasing P limitation, however, the total chlorophyll content decreased too, resulting in an exponential increase of the transmittance at 685 nm that indicates reduced reabsorption effects on F_{685}. We assume that due to the exponential increase in transmittance, $F_{\uparrow 685}$ increases more strongly than $F_{\uparrow 740}$, resulting in an increase in the $F_{\uparrow ratio}$ with intensifying P limitation (c.f. Figure 7). Correcting $F_{\uparrow 685}$ for these effects using the exponential relationship between the transmittance at 685 nm with $CI_{red\text{-}edge}$, resulted in a strong linear relationship between $cF_{\uparrow ratio}$ and Φ_{PSII}. This supports our fourth hypothesis that due to the changing contribution of PSII and PSI under P limitation the

518 $cF_{\uparrow ratio}$ can be linked to Φ_{PSII}. At the leaf level, the $cF_{\uparrow ratio}$ was a precise and accurate
519 predictor of Φ_{PSII}, which is of particular interest since the $cF_{\uparrow ratio}$, in contrast to F_{norm}, does
520 not need to be normalized by green APAR. Satellite based green APAR depends on
521 reflectance based estimations of fPAR, which is in particular challenging in ecosystems
522 where the reflectance does not drop when photosynthesis is decoupled from greenness
523 (Joiner *et al.*, 2014). Therefore the $cF_{\uparrow ratio}$ might be better suited for satellite applications
524 than F_{norm}. At canopy level, however, the estimation of photosynthetic parameters by
525 $cF_{\uparrow ratio}$ comes with several challenges which have to be addressed in future studies: i) the
526 relationship of transmittance and $CI_{red\text{-}edge}$ is likely species dependent, ii) structural effects
527 will complicate the correction for reduced reabsorption effects at canopy level (Liu & Liu,
528 2018; Romero *et al.*, 2020), iii) the retrieval of red SIF at canopy level comes with a lower
529 signal quality than far-red SIF.
530 Our results are in agreement with previous studies showing that upward emitted F_{norm}
531 can contribute up to 65% to total leaf F_{norm} (Van Wittenberghe *et al.*, 2013, 2015). We
532 also showed that the contribution of $F_{\uparrow}$ to F_{tot} ($F_{\uparrow\%}$) decreased from 65% to 48% under P
533 limitation. For observations at canopy or ecosystem scale, this implies that under P limited
534 conditions an increased amount of fluorescence is emitted by the lower side of the leaf,
535 affecting the reabsorption intensity and scattering directions within the canopy. We
536 hypothesize that the changing $F_{\uparrow\%}$ under P limitation can be caused by two processes.
537 First, red fluorescence is partly reabsorbed by the foliar light harvesting complexes (Van
538 Wittenberghe *et al.*, 2015). With decreasing total chlorophyll under P limitation, more red
539 fluorescence is transmitted through the leaf, increasing red $F_{\downarrow}$ and thus decreasing $F_{\uparrow\%}$
540 (Figure S4). However, the coincident decrease of far-red $F_{\uparrow\%}$, which is less affected by
541 reabsorption and mostly scattered by internal structures of the leaf (Louis *et al.*, 2006),
542 indicates that a mechanism independent of reabsorption decreased $F_{\uparrow\%}$ under P limited
543 conditions. An alternative explanation may be related to chloroplasts moving from the
544 cell surface to the side walls of cells to protect against excessive energy, thereby
545 decreasing the fraction of light that is absorbed (Kasahara *et al.*, 2002). The chloroplast

avoidance movement and the subsequent realignment of the light harvesting complexes may affect F emission and direction of scattering within the leaf, decreasing the fraction of F escaping from the upper surface of the leaf.

In this study we focused on the estimation of the quantum use efficiency, an essential indicator for the efficiency of the light reactions and more closely linked to fluorescence than fluorescence is to the Calvin cycle. Further experimental work combining multiple sensors and measurement techniques at leaf and canopy are essential to better elucidate the links between fluorescence-derived remote sensing indices and photosynthesis. Such studies should address i) under which environmental conditions the relationship between F_{norm} and Φ_{PSII} changes and how relevant this might be for satellite observations; ii) if canopy F_{ratio} can be universally corrected for reabsorption effects and; iii) if this allows an improved estimation of photosynthetic activity from different sensor platforms.

Conclusion

We examined the relationship between total fluorescence and gross photosynthesis as well as the relationship between F_{norm}, F_{ratio} and the PRI to the quantum efficiency of PSII (Φ_{PSII}) along a P limitation gradient at leaf level. We demonstrate that under stable light conditions the relationship between total fluorescence and gross photosynthesis was not linear across a P gradient. We show that Φ_{PSII} cannot be predicted from F_{norm} alone due to the non-monotonic relationship between the two variables. We demonstrate, however, that the pigment corrected $cPRI_{vi}$ and $cF_{\uparrow ratio}$ share both a strong linear relationship with Φ_{PSII}, thereby enabling the estimation of Φ_{PSII} at leaf level. The advantage of one predictors over the other depends mainly on their scalability. While, the $cPRI_{vi}$ requires information about Chl:Car ratio, the $cF_{\uparrow ratio}$ depends only on Chl content, which can facilitate the upscaling.

The possibility to compensate for reabsorption effects at foliar level as demonstrated in this study can help to improve F_{ratio} estimations. This might allow predicting light use efficiency without the need of measuring green APAR. Our results imply that overlooking

574 the physiological status of vegetation may result in a misinterpretation of the SIF signal,
575 introducing errors in photosynthesis estimates. With the growing SIF research community
576 and the increasing range of applications at global scale, we would also like to stress the
577 importance of SIF measurements at leaf level. SIF measured at the leaf level will help to
578 avoid misinterpretations of canopy signals and will help to improve our understanding of
579 the changing relationships between F_{norm} and photochemical- and non-photochemical
580 quenching, under different environmental conditions.
581
582 **Acknowledgments**
583 This research was supported by the Research Foundation—Flanders (FWO) G0D5415N,
584 by the European Research Council grant ERCSyG-610028 IMBALANCE-P and by
585 Methusalem funding of the Research Council UA. Sebastian Wieneke has received funding
586 from the European Union Horizon 2020 Research and Innovation program under the
587 Marie Skłodowska-Curie grant (ReSPEc, grant no 795299). Manuela Balzarolo has received
588 funding from the European Union Horizon 2020 Research and Innovation program under
589 the Marie Skłodowska-Curie grant (INDRO, grant no 702717). Hamada AbdElgawad is a
590 postdoctoral researcher of the Research Foundation – Flanders (FWO; 12U8918N).
591
592 **Author Contributions**
593 SW, MB, SV designed the experiment and the research, SW, MB, AV, MSV conducted the
594 measurements, HA, HAE performed the laboratory analysis, SV, IAJ, JP, UR, HA, HAE, MB,
595 AV, MSV conducted review, editing and provided expert advice in different stages of the
596 study, SV and IAJ provided funding acquisition, project administration, and resources, SW
597 wrote the paper.
598
599 **References**

Alonso L, Van Wittenberghe S, Amorós-López J, Vila-Francés J, Gómez-Chova L, Moreno J. **2017**. Diurnal Cycle Relationships between Passive Fluorescence, PRI and NPQ of Vegetation in a Controlled Stress Experiment. *Remote Sensing* **9**: 770.

Baker NR. **2008**. Chlorophyll Fluorescence: A Probe of Photosynthesis In Vivo. *Annual Review of Plant Biology* **59**: 89–113.

Balzarolo M, Peñuelas J, Filella I, Portillo-Estrada M, Ceulemans R. **2018**. Assessing Ecosystem Isoprene Emissions by Hyperspectral Remote Sensing. *Remote Sensing* **10**: 1086.

Buschmann C. **2007**. Variability and application of the chlorophyll fluorescence emission ratio red/far-red of leaves. *Photosynthesis Research* **92**: 261–271.

Carstensen A, Herdean A, Schmidt SB, Sharma A, Spetea C, Pribil M, Husted S. **2018**. The impacts of phosphorus deficiency on the photosynthetic electron transport chain. *Plant Physiology*: pp.01624.2017.

Ciais P, Sabine C, Bala G, Bopp L, Brovkin V, Canadell J, Chhabra A, DeFries R, Galloway J, Heimann M, *et al.* 2014. Carbon and other biogeochemical cycles. In: Climate change 2013: the physical science basis. Contribution of Working Group I to the Fifth Assessment Report of the Intergovernmental Panel on Climate Change. Cambridge University Press, 465–570.

Conroy JP, Smillie RM, Küppers M, Bevege DI, Barlow EW. **1986**. Chlorophyll a Fluorescence and Photosynthetic and Growth Responses of Pinus radiata to Phosphorus Deficiency, Drought Stress, and High CO2. *Plant Physiology* **81**: 423–429.

Dechant B, Ryu Y, Badgley G, Zeng Y, Berry JA, Zhang Y, Goulas Y, Li Z, Zhang Q, Kang M, *et al.* 2020. Canopy structure explains the relationship between photosynthesis and sun-induced chlorophyll fluorescence in crops. *Remote Sensing of Environment* **241**: 111733.

Filella I, Porcar-Castell A, Munné-Bosch S, Bäck J, Garbulsky MF, Peñuelas J. **2009**. PRI assessment of long-term changes in carotenoids/chlorophyll ratio and short-term changes in de-epoxidation state of the xanthophyll cycle. *International Journal of Remote Sensing* **30**: 4443–4455.

Frankenberg C, Fisher JB, Worden J, Badgley G, Saatchi SS, Lee J-E, Toon GC, Butz A, Jung M, Kuze A, *et al.* 2011. New global observations of the terrestrial carbon cycle from GOSAT: Patterns of plant fluorescence with gross primary productivity. *Geophysical Research Letters* **38**: L17706.

Frydenvang J, Maarschalkerweerd M van, Carstensen A, Mundus S, Schmidt SB, Pedas PR, Laursen KH, Schjoerring JK, Husted S. **2015**. Sensitive Detection of Phosphorus Deficiency in Plants Using Chlorophyll a Fluorescence. *Plant Physiology* **169**: 353–361.

Gamon JA, Field CB, Fredeen AL, Thayer S. **2001**. Assessing photosynthetic downregulation in sunflower stands with an optically-based model. *Photosynthesis Research* **67**: 113–125.

Gamon JA, Peñuelas J, Field CB. **1992**. A narrow-waveband spectral index that tracks diurnal changes in photosynthetic efficiency. *Remote Sensing of Environment* **41**: 35–44.

Garbulsky MF, Peñuelas J, Gamon J, Inoue Y, Filella I. **2011**. The photochemical reflectance index (PRI) and the remote sensing of leaf, canopy and ecosystem radiation use efficiencies: A review and meta-analysis. *Remote Sensing of Environment* **115**: 281–297.

Ge Z, Rubio G, Lynch JP. **2000**. The importance of root gravitropism for inter-root competition and phosphorus acquisition efficiency: results from a geometric simulation model. *Plant and Soil* **218**: 159–171.

Genty B, Briantais J-M, Baker NR. **1989**. The relationship between the quantum yield of photosynthetic electron transport and quenching of chlorophyll fluorescence. *Biochimica et Biophysica Acta (BBA) - General Subjects* **990**: 87–92.

Giovannetti M, Mosse B. **1980**. An Evaluation of Techniques for Measuring Vesicular Arbuscular Mycorrhizal Infection in Roots. *New Phytologist* **84**: 489–500.

Gitelson A. **2020**. Towards a generic approach to remote non-invasive estimation of foliar carotenoid-to-chlorophyll ratio. *Journal of Plant Physiology* **252**: 153227.

Gitelson AA, Gamon JA, Solovchenko A. **2017a**. Multiple drivers of seasonal change in PRI: Implications for photosynthesis 1. Leaf level. *Remote Sensing of Environment* **191**: 110–116.

Gitelson AA, Gamon JA, Solovchenko A. **2017b**. Multiple drivers of seasonal change in PRI: Implications for photosynthesis 2. Stand level. *Remote Sensing of Environment* **190**: 198–206.

Gitelson AA, Gritz † Y, Merzlyak MN. **2003**. Relationships between leaf chlorophyll content and spectral reflectance and algorithms for non-destructive chlorophyll assessment in higher plant leaves. *Journal of Plant Physiology* **160**: 271–282.

Gitelson AA, Keydan GP, Merzlyak MN. **2006**. Three-band model for noninvasive estimation of chlorophyll, carotenoids, and anthocyanin contents in higher plant leaves. *Geophysical Research Letters* **33**.

Guanter L, Zhang Y, Jung M, Joiner J, Voigt M, Berry JA, Frankenberg C, Huete AR, Zarco-Tejada P, Lee J-E, *et al.* 2014. Global and time-resolved monitoring of crop photosynthesis with chlorophyll fluorescence. *Proceedings of the National Academy of Sciences* **111**: E1327–E1333.

Harris CR, Millman KJ, van der Walt SJ, Gommers R, Virtanen P, Cournapeau D, Wieser E, Taylor J, Berg S, Smith NJ, *et al.* 2020. Array programming with NumPy. *Nature* **585**: 357–362.

Hou E, Wen D, Jiang L, Luo X, Kuang Y, Lu X, Chen C, Allen KT, He X, Huang X, *et al.* 2021. Latitudinal patterns of terrestrial phosphorus limitation over the globe. *Ecology Letters* **24**: 1420–1431.

Joiner J, Yoshida Y, Vasilkov AP, Schaefer K, Jung M, Guanter L, Zhang Y, Garrity S, Middleton EM, Huemmrich KF, *et al.* 2014. The seasonal cycle of satellite chlorophyll fluorescence

observations and its relationship to vegetation phenology and ecosystem atmosphere carbon exchange. *Remote Sensing of Environment* **152**: 375–391.

Kasahara M, Kagawa T, Oikawa K, Suetsugu N, Miyao M, Wada M. **2002**. Chloroplast avoidance movement reduces photodamage in plants. *Nature* **420**: 829.

Kohzuma K, Hikosaka K. **2018**. Physiological validation of photochemical reflectance index (PRI) as a photosynthetic parameter using Arabidopsis thaliana mutants. *Biochemical and Biophysical Research Communications* **498**: 52–57.

Liao H, Rubio G, Yan X, Cao A, Brown KM, Lynch JP. **2001**. Effect of phosphorus availability on basal root shallowness in common bean. *Plant and Soil* **232**: 69–79.

Lichtenthaler HK, Rinderle U. **1988**. The Role of Chlorophyll Fluorescence in The Detection of Stress Conditions in Plants. *C R C Critical Reviews in Analytical Chemistry* **19**: S29–S85.

Lima JD, Mosquim PR, Da Matta FM. **1999**. Leaf Gas Exchange and Chlorophyll Fluorescence Parameters in Phaseolus Vulgaris as Affected by Nitrogen and Phosphorus Deficiency. *Photosynthetica* **37**: 113–121.

Liu X, Liu L. **2018**. Influence of the canopy BRDF characteristics and illumination conditions on the retrieval of solar-induced chlorophyll fluorescence. *International Journal of Remote Sensing* **39**: 1782–1799.

Louis J, Cerovic ZG, Moya I. **2006**. Quantitative study of fluorescence excitation and emission spectra of bean leaves. *Journal of Photochemistry and Photobiology B: Biology* **85**: 65–71.

Magney TS, Barnes ML, Yang X. **2020**. On the Covariation of Chlorophyll Fluorescence and Photosynthesis Across Scales. *Geophysical Research Letters* **47**: e2020GL091098.

Magney TS, Bowling DR, Logan BA, Grossmann K, Stutz J, Blanken PD, Burns SP, Cheng R, Garcia MA, Köhler P, *et al.* 2019. Mechanistic evidence for tracking the seasonality of photosynthesis with solar-induced fluorescence. *Proceedings of the National Academy of Sciences* **116**: 11640–11645.

Magney Troy S., Frankenberg Christian, Fisher Joshua B., Sun Ying, North Gretchen B., Davis Thomas S., Kornfeld Ari, Siebke Katharina. **2017**. Connecting active to passive fluorescence with photosynthesis: a method for evaluating remote sensing measurements of Chl fluorescence. *New Phytologist* **215**: 1594–1608.

Maguire AJ, Eitel JUH, Griffin KL, Magney TS, Long RA, Vierling LA, Schmiege SC, Jennewein JS, Weygint WA, Boelman NT, *et al.* 2020. On the Functional Relationship Between Fluorescence and Photochemical Yields in Complex Evergreen Needleleaf Canopies. *Geophysical Research Letters* **47**: e2020GL087858.

Marrs JK, Reblin JS, Logan BA, Allen DW, Reinmann AB, Bombard DM, Tabachnik D, Hutyra LR. **2020**. Solar-Induced Fluorescence Does Not Track Photosynthetic Carbon Assimilation Following Induced Stomatal Closure. *Geophysical Research Letters* **47**: e2020GL087956.

Marschner H, Römheld V, Horst WJ, Martin P. **1986**. Root-induced changes in the rhizosphere: Importance for the mineral nutrition of plants. *Zeitschrift für Pflanzenernährung und Bodenkunde* **149**: 441–456.

Maxwell K, Johnson GN. **2000**. Chlorophyll fluorescence—a practical guide. *Journal of Experimental Botany* **51**: 659–668.

McKinney W. **2010**. Data Structures for Statistical Computing in Python. *Proceedings of the 9th Python in Science Conference*: 56–61.

Meroni M, Rossini M, Guanter L, Alonso L, Rascher U, Colombo R, Moreno J. **2009**. Remote sensing of solar-induced chlorophyll fluorescence: Review of methods and applications. *Remote Sensing of Environment* **113**: 2037–2051.

Merzlyak MN, Gitelson AA, Chivkunova OB, Rakitin VY. **1999**. Non-destructive optical detection of pigment changes during leaf senescence and fruit ripening. *Physiologia Plantarum* **106**: 135–141.

Miao G, Kaiyu G, Xi Y, J. BC, A. BJ, H. DE, Jin W, E. MC, Katherine M, Yaping C, *et al.* 2018. Sun-Induced Chlorophyll Fluorescence, Photosynthesis, and Light Use Efficiency of a Soybean Field from Seasonally Continuous Measurements. *Journal of Geophysical Research: Biogeosciences* **123**: 610–623.

Migliavacca M, Perez-Priego O, Rossini M, El-Madany TS, Moreno G, van der Tol C, Rascher U, Berninger A, Bessenbacher V, Burkart A, *et al.* 2017. Plant functional traits and canopy structure control the relationship between photosynthetic CO2 uptake and far-red sun-induced fluorescence in a Mediterranean grassland under different nutrient availability. *New Phytologist*: n/a-n/a.

Mohammed GH, Colombo R, Middleton EM, Rascher U, van der Tol C, Nedbal L, Goulas Y, Pérez-Priego O, Damm A, Meroni M, *et al.* 2019. Remote sensing of solar-induced chlorophyll fluorescence (SIF) in vegetation: 50 years of progress. *Remote Sensing of Environment* **231**: 111177.

Müller P, Li X-P, Niyogi KK. **2001**. Non-Photochemical Quenching. A Response to Excess Light Energy. *Plant Physiology* **125**: 1558–1566.

Pedregosa F, Varoquaux G, Gramfort A, Michel V, Thirion B, Grisel O, Blondel M, Prettenhofer P, Weiss R, Dubourg V, *et al.* 2011. Scikit-learn: Machine Learning in Python. *Journal of Machine Learning Research* **12**: 2825–2830.

Penuelas J, Baret F, Filella I. **1995**. Semi-empirical indices to assess carotenoids/chlorophyll a ratio from leaf spectral reflectance. *Photosynthetica* **31**: 221–230.

Peñuelas J, Filella I, Gamon JA. **1995**. Assessment of photosynthetic radiation-use efficiency with spectral reflectance. *New Phytologist* **131**: 291–296.

Peñuelas J, Filella I, Gamon JA, Field C. **1997**. Assessing photosynthetic radiation-use efficiency of emergent aquatic vegetation from spectral reflectance. *Aquatic Botany* **58**: 307–315.

Peñuelas J, Gamon JA, Fredeen AL, Merino J, Field CB. **1994**. Reflectance indices associated with physiological changes in nitrogen- and water-limited sunflower leaves. *Remote Sensing of Environment* **48**: 135–146.

Peñuelas J, Garbulsky MF, Filella I. **2011**. Photochemical reflectance index (PRI) and remote sensing of plant CO2 uptake. *New Phytologist* **191**: 596–599.

Pinto F, Damm A, Schickling A, Panigada C, Cogliati S, Müller-Linow M, Balvora A, Rascher U. **2016**. Sun-induced chlorophyll fluorescence from high-resolution imaging spectroscopy data to quantify spatio-temporal patterns of photosynthetic function in crop canopies. *Plant, Cell & Environment* **39**: 1500–1512.

Porcar-Castell A, Garcia-Plazaola JI, Nichol CJ, Kolari P, Olascoaga B, Kuusinen N, Fernández-Marín B, Pulkkinen M, Juurola E, Nikinmaa E. **2012**. Physiology of the seasonal relationship between the photochemical reflectance index and photosynthetic light use efficiency. *Oecologia* **170**: 313–323.

Porcar-Castell A, Tyystjärvi E, Atherton J, Tol C van der, Flexas J, Pfündel EE, Moreno J, Frankenberg C, Berry JA. **2014**. Linking chlorophyll a fluorescence to photosynthesis for remote sensing applications: mechanisms and challenges. *Journal of Experimental Botany*: eru191.

Rahimzadeh-Bajgiran P, Munehiro M, Omasa K. **2012**. Relationships between the photochemical reflectance index (PRI) and chlorophyll fluorescence parameters and plant pigment indices at different leaf growth stages. *Photosynthesis Research* **113**: 261–271.

Rahman AF, Cordova VD, Gamon JA, Schmid HP, Sims DA. **2004**. Potential of MODIS ocean bands for estimating CO2 flux from terrestrial vegetation: A novel approach. *Geophysical Research Letters* **31**.

Romero JM, Cordon GB, Lagorio MG. **2020**. Re-absorption and scattering of chlorophyll fluorescence in canopies: A revised approach. *Remote Sensing of Environment* **246**: 111860.

Sims DA, Gamon JA. **2002**. Relationships between leaf pigment content and spectral reflectance across a wide range of species, leaf structures and developmental stages. *Remote Sensing of Environment* **81**: 337–354.

Sun Y, Frankenberg C, Jung M, Joiner J, Guanter L, Köhler P, Magney T. **2018**. Overview of Solar-Induced chlorophyll Fluorescence (SIF) from the Orbiting Carbon Observatory-2: Retrieval, cross-mission comparison, and global monitoring for GPP. *Remote Sensing of Environment*.

Thayer SS, Björkman O. **1990**. Leaf Xanthophyll content and composition in sun and shade determined by HPLC. *Photosynthesis Research* **23**: 331–343.

van der Tol C, Berry JA, Campbell PKE, Rascher U. **2014**. Models of fluorescence and photosynthesis for interpreting measurements of solar induced chlorophyll fluorescence. *Journal of Geophysical Research: Biogeosciences*: 2014JG002713.

Van Wittenberghe S, Alonso L, Verrelst J, Hermans I, Delegido J, Veroustraete F, Valcke R, Moreno J, Samson R. **2013**. Upward and downward solar-induced chlorophyll fluorescence yield indices of four tree species as indicators of traffic pollution in Valencia. *Environmental Pollution* **173**: 29–37.

Van Wittenberghe S, Alonso L, Verrelst J, Moreno J, Samson R. **2015**. Bidirectional sun-induced chlorophyll fluorescence emission is influenced by leaf structure and light scattering properties — A bottom-up approach. *Remote Sensing of Environment* **158**: 169–179.

Ven A, Verlinden MS, Fransen E, Olsson PA, Verbruggen E, Wallander H, Vicca S. **2020**. Phosphorus addition increased carbon partitioning to autotrophic respiration but not to biomass production in an experiment with Zea mays. *Plant, Cell & Environment* **n/a**.

Verlinden MS, Ven A, Verbruggen E, Janssens IA, Wallander H, Vicca S. **2018**. Favorable effect of mycorrhizae on biomass production efficiency exceeds their carbon cost in a fertilization experiment. *Ecology* **99**: 2525–2534.

Vicca S, Balzarolo M, Filella I, Granier A, Herbst M, Knohl A, Longdoz B, Mund M, Nagy Z, Pintér K, *et al.* 2016. Remotely-sensed detection of effects of extreme droughts on gross primary production. *Scientific Reports* **6**: 28269.

Vierheilig H, Schweiger P, Brundrett M. **2005**. An overview of methods for the detection and observation of arbuscular mycorrhizal fungi in roots†. *Physiologia Plantarum* **125**: 393–404.

Virtanen P, Gommers R, Oliphant TE, Haberland M, Reddy T, Cournapeau D, Burovski E, Peterson P, Weckesser W, Bright J, *et al.* 2020. SciPy 1.0: fundamental algorithms for scientific computing in Python. *Nature Methods* **17**: 261–272.

Wieneke S, Burkart A, Cendrero-Mateo MP, Julitta T, Rossini M, Schickling A, Schmidt M, Rascher U. **2018**. Linking photosynthesis and sun-induced fluorescence at sub-daily to seasonal scales. *Remote Sensing of Environment* **219**: 247–258.

Wohlfahrt G, Gerdel K, Migliavacca M, Rotenberg E, Tatarinov F, Müller J, Hammerle A, Julitta T, Spielmann FM, Yakir D. **2018**. Sun-induced fluorescence and gross primary productivity during a heat wave. *Scientific Reports* **8**: 14169.

Wong CYS, Gamon JA. **2015**. Three causes of variation in the photochemical reflectance index (PRI) in evergreen conifers. *New Phytologist* **206**: 187–195.

Wood JD, Griffis TJ, Baker JM, Frankenberg C, Verma M, Yuen K. **2017**. Multiscale analyses of solar-induced florescence and gross primary production. *Geophysical Research Letters* **44**: 2016GL070775.

Woodgate W, Suarez L, van Gorsel E, Cernusak LA, Dempsey R, Devilla R, Held A, Hill MJ, Norton AJ. **2019**. tri-PRI: A three band reflectance index tracking dynamic photoprotective mechanisms in a mature eucalypt forest. *Agricultural and Forest Meteorology* **272–273**: 187–201.

Yang K, Ryu Y, Dechant B, Berry JA, Hwang Y, Jiang C, Kang M, Kim J, Kimm H, Kornfeld A, *et al.* 2018. Sun-induced chlorophyll fluorescence is more strongly related to absorbed light than to photosynthesis at half-hourly resolution in a rice paddy. *Remote Sensing of Environment* **216**: 658–673.

Yang X, Tang J, Mustard JF, Lee J-E, Rossini M, Joiner J, Munger JW, Kornfeld A, Richardson AD. **2015**. Solar-induced chlorophyll fluorescence that correlates with canopy photosynthesis on diurnal and seasonal scales in a temperate deciduous forest. *Geophysical Research Letters* **42**: 2015GL063201.

Yaryura P, Cordon G, Leon M, Kerber N, Pucheu N, Rubio G, García A, Lagorio MG. **2009**. Effect of Phosphorus Deficiency on Reflectance and Chlorophyll Fluorescence of Cotyledons of Oilseed Rape (Brassica napus L.). *Journal of Agronomy and Crop Science* **195**: 186–196.

Zhang C, Filella I, Liu D, Ogaya R, Llusià J, Asensio D, Peñuelas J. **2017**. Photochemical Reflectance Index (PRI) for Detecting Responses of Diurnal and Seasonal Photosynthetic Activity to Experimental Drought and Warming in a Mediterranean Shrubland. *Remote Sensing* **9**: 1189.

Zhang Q, Wang YP, Pitman AJ, Dai YJ. **2011**. Limitations of nitrogen and phosphorous on the terrestrial carbon uptake in the 20th century. *Geophysical Research Letters* **38**: L22701.

Zhou X, Huang W, Kong W, Ye H, Dong Y, Casa R. **2017**. Assessment of leaf carotenoids content with a new carotenoid index: Development and validation on experimental and model data. *International Journal of Applied Earth Observation and Geoinformation* **57**: 24–35.

Zhou X, Huang W, Zhang J, Kong W, Casa R, Huang Y. **2019**. A novel combined spectral index for estimating the ratio of carotenoid to chlorophyll content to monitor crop physiological and phenological status. *International Journal of Applied Earth Observation and Geoinformation* **76**: 128–142.

Supplementary data

Mycorrhizal colonization

In both campaigns, mycorrhizal colonization in roots was verified in July and August by sampling roots from two plants per mesocosm. Per plant, 20 cm of one lateral root containing root hair was excavated, cut and stored at 5 °C for maximum two days. These roots were cleared and stained using a non-vital staining technique (as described by Vierheilig et al., 2005), using a 5% KOH-solution and a Sheaffer Black Ink solution (10% ink in a 10% acetic acid solution). The roots were transferred to a microscope slide and mycorrhizal colonization was quantified by counting arbuscules, vesicles and hyphae applying the gridline intersection method (Giovannetti & Mosse, 1980; Vierheilig *et al.*, 2005) (Figure S1a).

Table S1: Average (mean) and standard error (SE) of mycorrhizal colonization in roots, expressed as % of roots colonized by hyphae, arbuscules or vesicules for each treatment one and two months after planting. p values from a linear regression show P fertilization effect.

mycorrhizal colonization in roots

treatment	*hyphae*		*arbuscules*		*vesicles*	
	%		*%*		*%*	
	one month after planting					
	mean	*se*	*mean*	*se*	*mean*	*se*
P1	18.6	3.8	2.4	0.8	2	1.2
P2	13.4	4.3	2.4	1.5	1	0.6
P3	33.6	6.7	11.8	3.6	5.8	2.1
P4	28.5	7.3	11.1	3.9	5.2	2
P1_noAMF	0	0	0	0	0	0
P4_noAMF	0	0	0	0	0	0
P fertilization effect	NA		NA		NA	
P fertilization effect	p = 0.18		p = 0.14		p = 0.23	
	two months after planting					
	mean	*se*	*mean*	*se*	*mean*	*se*
P1	50.4	6.6	11.6	3.1	20	6.2
P2	35.6	11.1	7.2	3.7	11.6	5.5
P3	53.2	5.2	9.2	2.4	14	2.2
P4	63.7	9	22.1	5.8	28.5	7
P1_noAMF	0	0	0	0	0	0

P4_noAMF	0	0	0	0	0	0
P fertilization effect	p < 0.01		p < 0.01		p < 0.01	
P fertilization effect	p = 0.08		p = 0.03		p = 0.13	

851

852

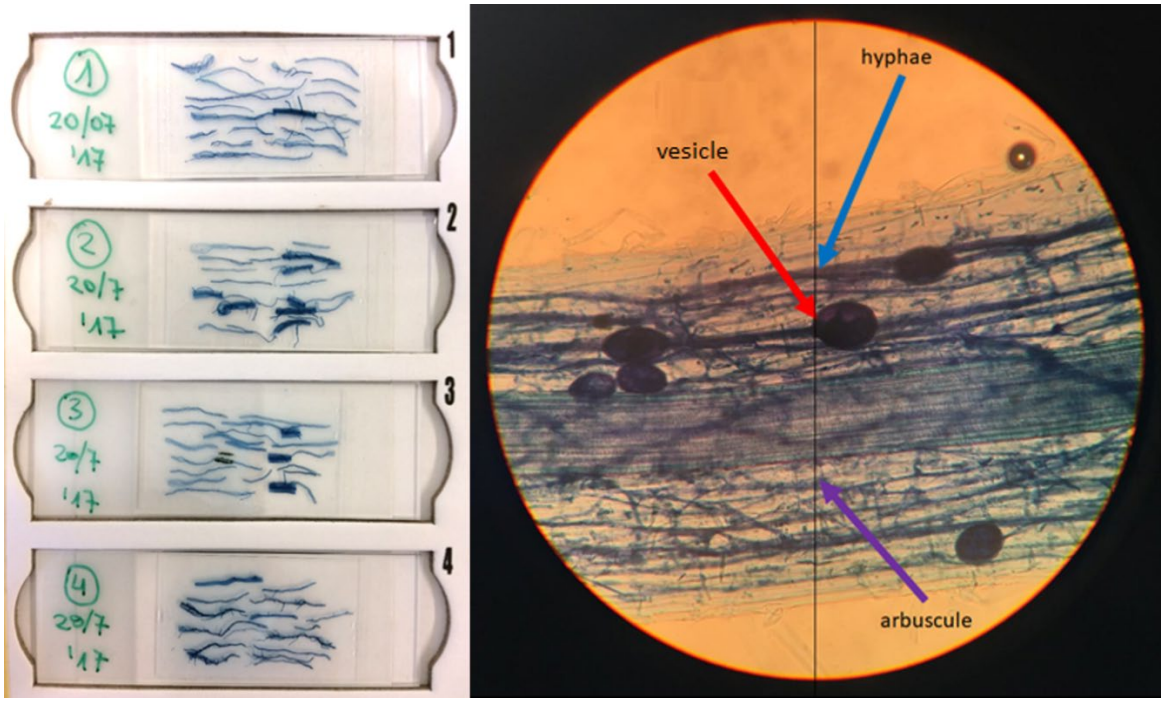

Figure S1: (left) Four microscope slides with root pieces. (right) A microscope view on a stained maize root containing a lot of AMF arbuscules, vesicles and hyphae. Each arrow goes to the first of a kind of AMF structure crossing the gridline (from above to below).

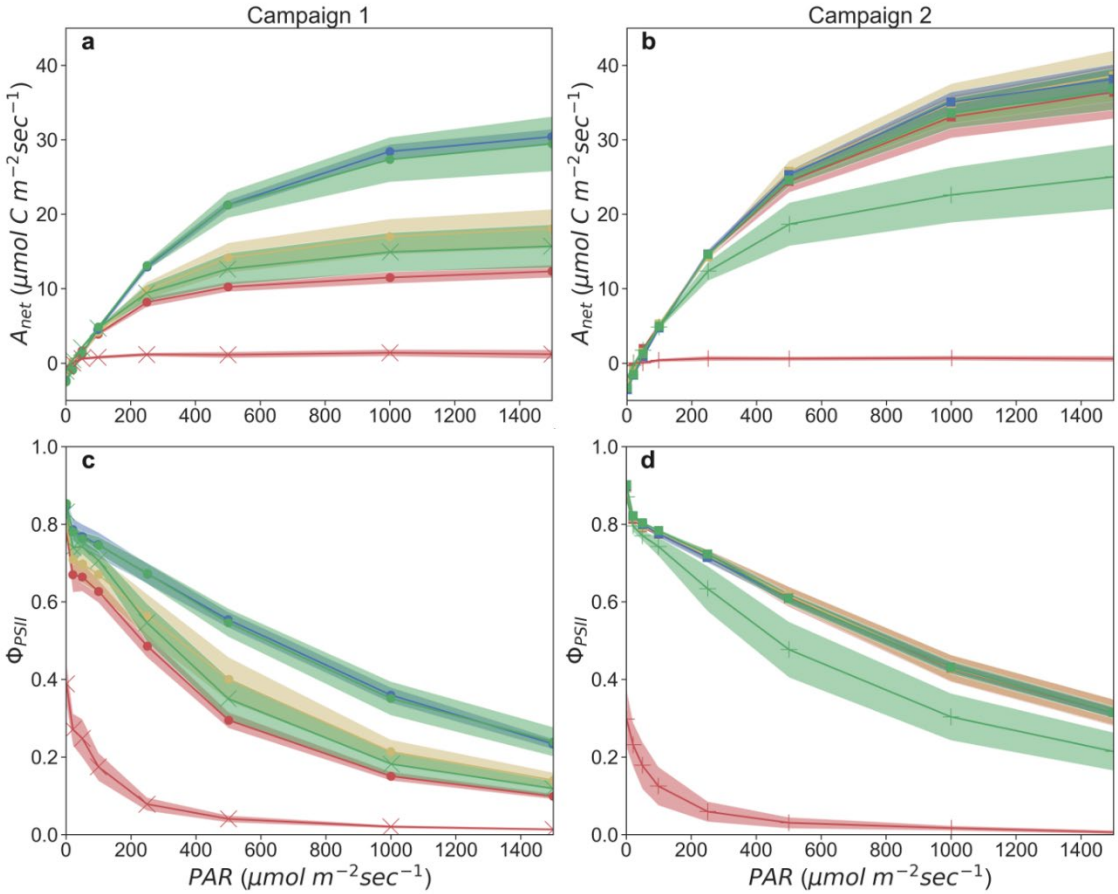

Figure S2: Averaged light response curves of the six different treatments measured during campaign one (a) and campaign two (b). Dot colors represent the treatments (green, P4; blue, P3; yellow, P2; red, P1), and the crosses represent the treatments without arbuscular mycorrhizal fungi (P4S, P1S). P1, P2, P3 and P4 indicate treatment with 2.5, 5, 10 and 20 kg P ha-1 triple superphosphate, respectively. P1S and P4S were pasteurized to ensure the absence of arbuscular mycorrhizal fungi.

Composition of foliar pigments under P limitation

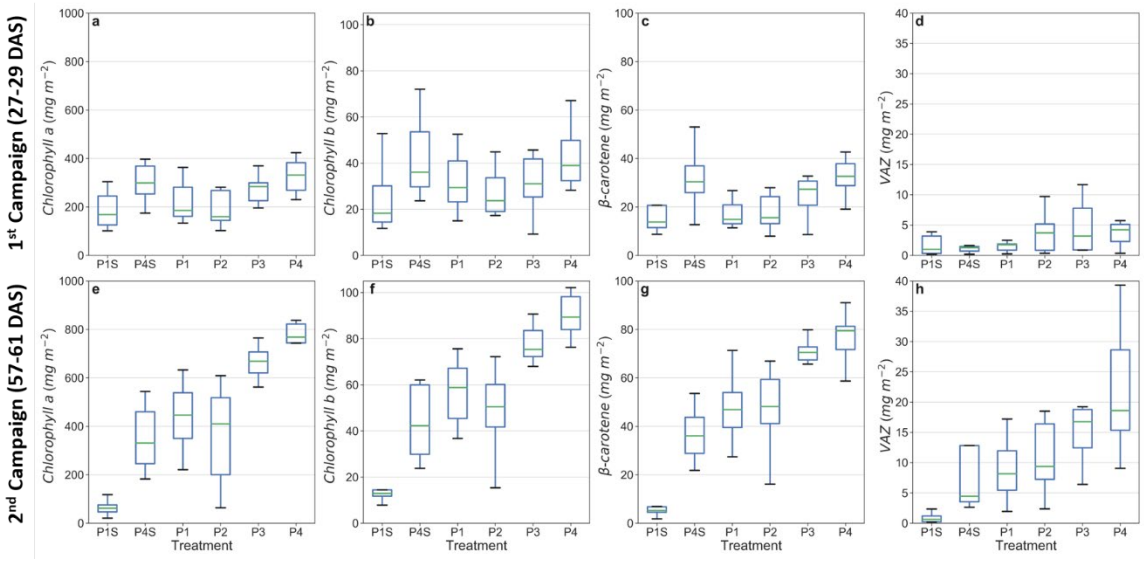

Figure S3: Box plots of chlorophyll a , chlorophyll b, β-carotene and the total xanthophyll pigment (VAZ) content 27-29 days after seeding (DAS, first campaign) a-d, and 57-61 DAS (second campaign) e-h. P1, P2, P3 and P4 indicate treatment with 2.5, 5, 10 and 20 kg P ha-1 triple superphosphate, respectively. P1S and P4S were pasteurized to ensure the absence of arbuscular mycorrhizal fungi.

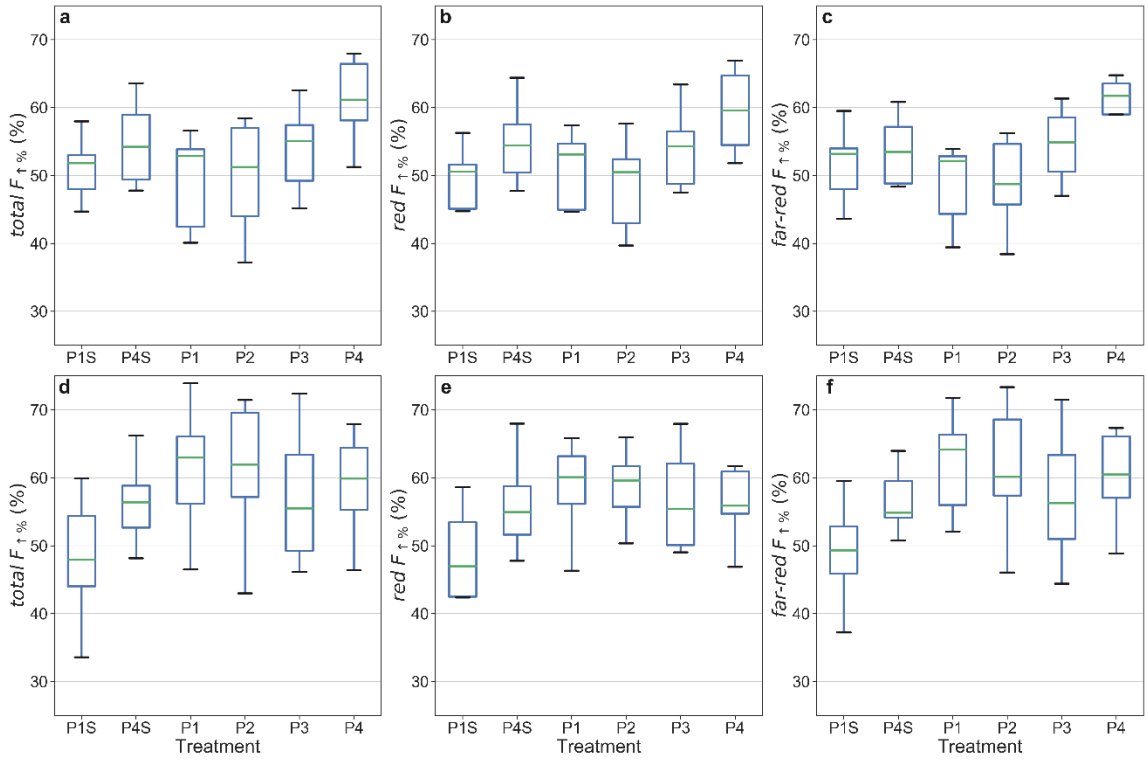

Figure S4: Box plots of the contribution of upward emitted red , far-red and total sun-induced fluorescence ($F_{\uparrow\%}$). a, b & c 27-29 days after seeding (first campaign), d, e & f 57-61 days after seeding (second campaign). P1, P2, P3 and P4 indicate treatment with 2.5, 5, 10 and 20 kg P ha-1 triple superphosphate, respectively. P1S and P4S were pasteurized to ensure the absence of arbuscular mycorrhizal fungi.

*Table S2: Spectral indices used in this study to estimate carotenoid to total chlorophyll ratio (Car:Chl). The asterisk indicate the two-tailed significance level (ns = P > 0.05, * = P ≤ 0.05, ** = P ≤ 0.01, *** = P ≤ 0.001).*

Spectral Index	Target variable	Model	R^2	Formula	Reference
NPCI	Car:Chl	linear	0.47^{*}	$(R_{680}- R_{430})/(R_{680}+R_{430})$	(Peñuelas *et al.*, 1994)
SIPI	Car:Chl		0.05^{ns}	$(R_{800}-R_{445})/(R_{800}-R_{680})$	(Penuelas *et al.*, 1995)
PSRI	Car:Chl		0^{ns}	$(R_{680}-R_{500})*R_{750}$	(Merzlyak *et al.*, 1999)
$CARI/CI_{red-edge}$	Car:Chl	linear	0.3^{ns}	$((R_{720}-R_{521})/R_{521})/((R_{750}-R_{705})/R_{705})$	(Zhou *et al.*, 2019)
$CRI/CI_{red-edge}$	Car:Chl	linear	0.55^{**}	$((R_{510})^{-1}-(R_{700})^{-1})/((R_{750}-R_{705})/R_{705})$	(Gitelson, 2020)
$CAR_{red-edge}/CI_{red-edge}$	Car:Chl	linear	0.6^{***}	$((R_{510})^{-1}-(R_{700})^{-1}]\times R_{770})/((R_{750}-R_{705})/R_{705})$	This study

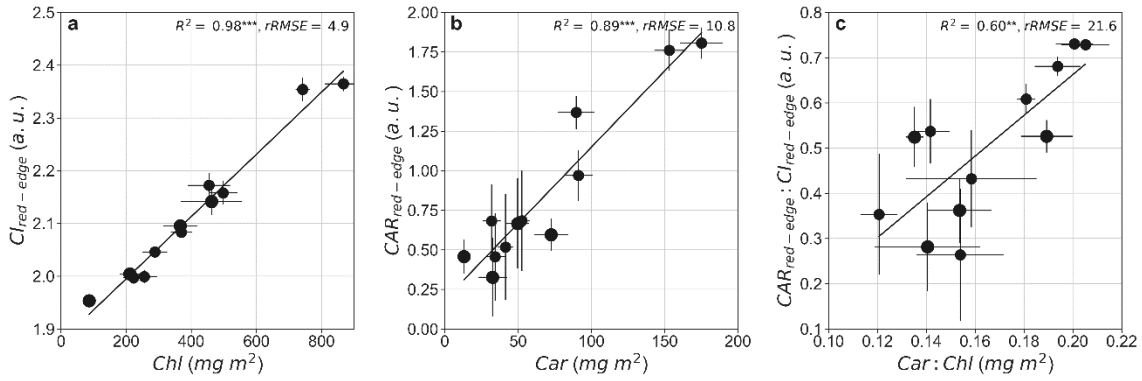

*Figure S5: (a) Relationship between the red-edge chlorophyll index (CIred-edge) and total chlorophyll content (Chl). (b) Relationship between the red-edge carotene index ($CAR_{red-edge}$) and carotene content (Car). (c) Relationship between the ratio of $CAR_{red-edge}$ to $CI_{red-edge}$ and the ratio of Car to Chl. The black line represents the best fitting model for all treatments for both campaigns. Dot colors represent the treatments (green, P4; blue, P3; yellow, P2; red, P1), and the crosses represent the treatments without arbuscular mycorrhizal fungi. The asterisk indicate the significance level (** = P ≤ 0.01, *** = P ≤ 0.001)*

*Table S3: Pearson coefficient (r) for the correlation of EPS, Car:Chl, sPRI, cPRI and $cPRI_{vi}$. The asterisk indicate the two-tailed significance level (ns = P > 0.05, * = P ≤ 0.05, ** = P ≤ 0.01, *** = P ≤ 0.001).*

	EPS	Car:Chl	sPRI	cPRI	$cPRI_{vi}$
EPS	1	0.743**	-0.753**	**-0.908*** **	-0.873***
Car:Chl	-	1	-0.479ns	-0.742**	-0.622**
sPRI	-	-	1	0.731**	0.902***
cPRI	-	-	-	1	0.9***
$cPRI_{vi}$	-	-	-	-	1

*Table S4: Pearson coefficient (r) for the partial correlation analysis of EPS, Car:Chl, sPRI, cPRI and $cPRI_{vi}$. The asterisk indicate the two-tailed significance level (ns = P > 0.05, * = P ≤ 0.05, ** = P ≤ 0.01, *** = P ≤ 0.001).*

		Correlation with EPS			
		Car:Chl	sPRI	cPRI	$cPRI_{vi}$
Control variables	Car:Chl	-	-0.676**	**-0.795*** **	-0.784***
	sPRI	0.662**	-	-	-
	cPRI	0.247ns	-	-	-
	$cPRI_{vi}$	0.523*	-	-	-